5-23-2019

Rapid In Situ Characterization of Soil Erodibility With a Field Deployable Robot

Feifei Qian
University of Pennsylvania, fqian@seas.upenn.edu

Dylan Lee
University of Pennsylvania, dylanblee@gmail.com

George Nikolich
Desert Research Institute

Daniel E. Koditschek
Electrical and Systems Engineering, University of Pennsylvania

Douglas J. Jerolmack
Earth and Environmental Science, University of Pennsylvania

Rapid In Situ Characterization of Soil Erodibility With a Field Deployable Robot

Abstract
Predicting the susceptibility of soil to wind erosion is difficult because it is a multivariate function of grain size, soil moisture, compaction, and biological growth. Erosive agents like plowing and grazing also differ in mechanism from entrainment by fluid shear; it is unclear if and how erosion thresholds for each process are related. Here we demonstrate the potential to rapidly assemble empirical maps of erodibility while also examining what controls it, using a novel "plowing" test of surface-soil shear resistance ($?_r$) performed by a semi-autonomous robot. Field work at White Sands National Monument, New Mexico, United States, examined gradients in erodibility at two scales: (i) soil moisture changes from dry dune crest to wet interdune (tens of meters) and (ii) downwind-increasing dune stabilization associated with growth of plants and salt and biological crusts (kilometers). We found that soil moisture changes of a few percent corresponded to a doubling of $?_r$, a result confirmed by laboratory experiments, and that soil crusts conferred stability that was comparable to moisture effects. We then compared different mechanisms of mechanical perturbation in a controlled laboratory setting. A new "kick-out" test determines peak shear resistance of the surface soil as a proxy for yield strength. Kick-out resistance exhibited a relation with soil moisture that was distinct from the plowing test and that was correlated with the independently measured threshold-fluid stress for wind erosion. Results show that our new method maps soil erodibility in arid environments and provides an understanding of environmental controls on variations in soil erodibility. (For more information: Kod*lab)

Keywords
legged robot, geomorphology, erodibility, shear strength

Disciplines
Electrical and Computer Engineering | Engineering | Systems Engineering

Rapid in-situ characterization of soil erodibility with a field deployable robot

Feifei Qian[1], Dylan Lee[2], George Nikolich[3], Daniel Koditschek[1], and Douglas Jerolmack[2,4]

Abstract.

Predicting the susceptibility of soil to wind erosion is difficult because it is a multivariate function of grain size, soil moisture, compaction, and biological growth. Erosive agents like plowing and grazing also differ in mechanism from entrainment by fluid shear; it is unclear if and how erosion thresholds for each process are related. Here we demonstrate the potential to rapidly assemble empirical maps of erodibility while also examining what controls it, using a novel "plowing" test of surface-soil shear resistance (τ_r) performed by a semi-autonomous robot. Field work at White Sands National Monument, New Mexico, USA, examined gradients in erodibility at two scales: (i) soil moisture changes from dry dune crest to wet interdune (10s m); and (ii) downwind-increasing dune stabilization associated with growth of plants, and salt and biological crusts (kilometers). We found that soil moisture changes of a few percent corresponded to a doubling of τ_r, a result confirmed by laboratory experiments, and that soil crusts conferred stability that was comparable to moisture effects. We then compared different mechanisms of mechanical perturbation in a controlled laboratory setting. A new "kick-out" test determines peak shear resistance of the surface soil as a proxy for yield strength. Kick-out resistance exhibited a relation with soil moisture that was distinct from the plowing test, and that was correlated with the independently measured threshold-fluid stress for wind erosion. Results show that our new method maps soil erodibility in arid environments and provides an understanding of environmental controls on variations in soil erodibility.

Key points:
1. A novel field method is presented that uses a robot's mechanical probing of soil to provide measurements of a soil's susceptibility to erosion.
2. Laboratory measurements are performed and compared to the field results to begin understanding the controls on erodibility in different parts of the dune field.
3. Initial field results lead us to develop other tests of soil erodibility that can provide an estimate of threshold wind-erosion stress.

1. Introduction

Human activities have accelerated the pace of desertification, directly through changes in land use and indirectly as a consequence of anthropogenic climate change [*Dai*, 2013; *Wu and Ci*, 2002; *Reich et al.*, 2001; *Yong-Zhong et al.*, 2005]. Increasing aridity increases the severity of dust storms, reduces net ecological productivity, and perturbs the biogeochemical cycle of the Earth [*Schlesinger et al.*, 1990; *Rosenfeld et al.*, 2001; *Loye-Pilot et al.*, 1986; *Goudie and Middleton*, 2001; *Dregne and Chou*, 1992]. A major contributor to enhanced dust emission in arid and semi-arid landscapes is changes to the erodibility of soil [*Bakker et al.*, 2008; *Yang et al.*, 2003], through mechanical disturbances such as grazing, off-road vehicle use, and agricultural activity [*Trimble and Mendel*, 1995; *Goossens and Buck*, 2009; *Van Oost et al.*, 2006]. These disturbances can induce soil compaction, changes in soil water content, alteration of infiltration patterns, and a decrease in vegetation [*Liddle and Grieg-Smith*, 1975; *Webb*, 1983; *Webb and Wilshire*, 2012; *Kutiel et al.*, 1999]).

The above considerations point to the importance of determining the resistance of soil to both intrusive shearing due to, e.g., plowing, and to normal forces from, e.g., grazing animals. Shear and normal resistance of soil are also important parameters for assessing vehicle navigability [*Bekker*, 1960; *Wong et al.*, 1989]. This mechanical resistance is dictated ultimately by inter-granular friction, which itself is a function of the rate and magnitude of loading [*Majmudar and Behringer*, 2005], degree of compaction [*Howell et al.*, 1999], size and shape of grains [*Santamarina and Cho*, 2004], degree of saturation [*Richefeu et al.*, 2006], vegetation [*Fattet et al.*, 2011], and effective cohesion [*Fredlund et al.*, 1996]. The critical fluid shear stress for wind entrainment, τ_c, also depends on these factors [*Chepil and Woodruff*, 1963]. For sand-sized particles, sediment flux is proportional to the boundary fluid-shear stress τ_b in excess of critical, $q \propto (\tau_b - \tau_c)$ [*Martin and Kok*, 2017]. Thus,

[1]Electrical and Systems Engineering, University of Pennsylvania, Philadelphia, PA, USA.
[2]Earth and Environmental Science, University of Pennsylvania, Philadelphia, PA, USA.
[3]Desert Research Institute, Division of Atmospheric Sciences, Las Vegas, NV, USA
[4]Mechanical Engineering and Applied Mechanics, University of Pennsylvania, Philadelphia, PA, USA.

0148-0227/19/$9.00

determining τ_c is essential for predicting if, and how much, erosion occurs for a given wind stress; it is also necessary for predicting dust emission, which is almost exclusively associated with sand saltation [*Kok et al.*, 2012]. Intuitively we expect that the mechanical resistance of soil, which we shall denote by some resisting stress τ_r, will be related somehow to the fluid threshold τ_c. It is not obvious, however, how the two might relate; wind entrainment involves turbulent flow impinging only on surficial grains, and high-impact collisions of saltating grains with the surface, while disturbances like plowing and stomping involve relatively slow deformation in the bulk of the soil bed.

In this paper we use the term "erodibility" to mean the inverse of a soil's resistance to deformation or erosion, be it a mechanical yield stress or a fluid threshold stress. Soil erodibility varies over a variety of spatial scales in arid environments, in response to myriad environmental controls. At the scale of 0.1 $\sim$ 3m the thickness and properties of desert crusts can display significant variability [*Belnap and Gillette*, 1998]. Plants are another factor at this scale, and feedbacks between desert crusts and plant life further introduce a codependence between vegetation and soil state [*Li et al.*, 2010, 2002]. Gradients in soil moisture can also be sharp in arid environments, where changes of a few percent may alter the wind erosion threshold by an order of magnitude [*Zender et al.*, 2003]. At the patch to landscape scale of 10m $\sim$ 10km, changes in plant type, communities, and density can have a dramatic effect on the net sediment transport rate through an area [*Breshears et al.*, 2009; *Wolfe and Nickling*, 1996]. Grain size may change across all scales, from sorting over a dune to downstream fining across an entire dune field [*Jerolmack et al.*, 2011]. In addition to this spatial variability, soil erodibility may vary in time in response to wetting/drying, land-use changes, and fires, among other factors [*Giovannini et al.*, 2001; *Celik*, 2005; *Cosentino et al.*, 2006; *Bakker et al.*, 2008]. Given the multivariate and potentially confounding environmental controls, erodibility must be measured empirically. Given the spatial and temporal heterogeneity in landscape structure, it is desirable to obtain rapid and highly spatially-resolved measurements; in other words, maps of erodibility that may be updated periodically.

Aeolian scientists have traditionally used *in-situ* wind tunnels to perform erosion tests [*Gillette*, 1978; *Gillette et al.*, 1980; *Shao et al.*, 1993]. This method is inherently limited in spatial resolution, however, primarily due to a lack of portability; this has also limited the deployment of such devices to a restricted number of field sites. More portable devices to assess the threshold wind stress τ_c have been developed recently [*Etyemezian et al.*, 2007; *Sweeney et al.*, 2008; *Goossens and Buck*, 2009], which have shown promise for the rapid assessment of erobility. Still, such devices must be deployed manually, and they do not assess the mechanical resistance τ_r of soil. A recently developed, semi-autonomous robotic platform holds the promise of being able to generate maps of soil erodibility, and even of vegetation cover/type [*Qian et al.*, 2017]. The advantage of this platform lies in its potential for rapid, automated data collection. Given that a paucity of data is one of the biggest factors limiting our knowledge of gradients in erodibility, it is sensible to seek to develop a method to test erodibility that takes advantage of this platform. This places constraints, however, on the size, weight, and mechanical configurations of any related device.

In this work, we propose a novel method to quickly and accurately characterize soil erodibility *in-situ*, by measuring the granular resistance force on a robotic leg as it shears through the surface layer of grains. We present the first laboratory and field results obtained using this method, and examine the controls of soil moisture and surface crusts on erodibility at White Sands National Monument, USA (Figure 1). We begin by introducing the details of our experimental protocols, followed by a demonstration of the capability of this platform to measure shear resistance and explore environmental controls at White Sands. Laboratory experiments are then used to isolate the control of soil moisture on shear resistance, and to confirm the validity of field measurements. We then perform controlled laboratory experiments to determine the resistance of soil to different perturbations, and find that a mechanical measure of yield strength with a robotic leg is a good proxy for the wind erosion threshold. Finally the potential of this method as a tool for examining the relative importance of different factors contributing to erodibility in the field is discussed.

2. Materials and Methods

2.1. Shear strength "Plowing" method

The foundation of the method used to characterize soil erodibility is the hypothesis that soil susceptibility to erosion and stability under external perturbations (such as vehicle disturbance, wind shear, etc.) can be characterized through measurements of mechanical shear strength of the substrate. This type of measurement was targeted because of its potential to be rapidly deployed by a robotic leg as it walks over a surface. In view of this goal, the shear strength measurements in this paper were performed by a direct-drive robotic leg [*Kenneally and Koditschek*, 2015] (Figure 2A, Figure 3A) consisting of two gearless motors [*Asada and Youcef-Toumi*, 1987] and a pair of symmetric five-bar aluminum leg links (total leg length 30 cm when fully extended). Because the leg actuators don't have gearboxes, they respond sensitively to external torques and forces [*Kenneally et al.*, 2016]. This allows us to accurately estimate the vertical (y axis) and horizontal (x axis) ground reaction forces exerted on the toe position using the leg kinematics [*Kenneally et al.*, 2016]. At each time point, the actual toe position recorded by the motor encoders was compared with the desired toe position determined by the programmed trajectory. The amount of force applied by the leg to the soil was estimated from this position deflection through the kinematics of the leg. The motors (T-Motor, U8) have a stall torque of 3.5 Nm, which allows outputting a shear force of > 15 N with a resolution of ≈ 0.01 N with the current configuration. The maximal force measurable depends on the position of the end-effector. In this study, we used the horizontal component of the leg force as a measure of soil shear strength. It has been demonstrated in the granular physics literature that bulk behaviors, such as the response of a granular media to shear and penetration, are qualitatively similar for a wide variety of materials [*Cho et al.*, 2006; *Li et al.*, 2013]. These similarities persist despite variations in the polydispersity and angularity of grains. These similarities allow us to apply the same shear and penetration resistance characterization method to a variety of soils, as well as use experimental results to provide insight on observations of the more complex granular systems found in the field.

In both lab and field experiments, the robotic leg performed a rectangular trajectory (Figure 2A, green arrows) to characterize the shear strength of the surface layer of the soil. At the beginning of each measurement, the direct-drive shear leg was submerged a small depth (a few centimeters) into the substrate, and subsequently dragged a thin layer of grains across the surface while recording the shear resistance force from the granular media. The leg then acted like a plow, pushing sand to the sides and front of the intruder. Figure 2B shows a sample measurement where the

robotic leg shears horizontally for 15cm with a shear speed of $u = 1$cm/s at a depth of $h = 4$cm. We calculated the shear strength of a soil at a certain depth as the average resistance force over the steady state range of the shear motion (shaded region in Figure 2B). An important issue to consider in performing such measurements is that the effective friction μ of a granular material varies with the dimensionless shear rate (Inertial number)

$$I = \dot{\gamma} D / \sqrt{P/\rho_p} \quad (1)$$

following the so-called '$\mu(I)$ rheology', where $\dot{\gamma} \approx u/h$ is shear rate, D is grain size, P is the (lithostatic) confining pressure and ρ_p is the particle density (see, e.g., [*Forterre and Pouliquen*, 2008; *Albert et al.*, 1999]). For $I < 10^{-3}$, however, granular flow is in the quasi-static regime where μ is — to first order — independent of I. All shear experiments in this study were performed with a shear rate of $u = 1$cm/s, much smaller than the rearranging speed $u_{rearrange} = \sqrt{2gd_g} \approx 10$cm/s [*Albert et al.*, 1999] for the granular material we used, and therefore the granular flow is within the quasi-static regime where we expect the effective friction coefficient to reflect only the static friction intrinsic to the granular medium.

2.1.1. Plowing field experiment

The field site we chose was White Sands National Monument in New Mexico, USA (see Figure 1). White Sands is a well-studied gypsum dune field located in the southwest of US that arises abruptly from a line source of sediment, has a well-defined dominant wind direction, and that features a shallow groundwater table which makes interdune surfaces moist — especially in the upwind portions of the dune field [*Langford*, 2003; *Kocurek et al.*, 2007; *Kocurek and Ewing*, 2005; *Reitz et al.*, 2010; *Jerolmack et al.*, 2012]. For the purposes of the study, the dune field can be thought of as being split into two primary regions. The first region is largely un-vegetated, has moist interdune surfaces that are within the capillary fringe, and is populated by transverse dunes that give way to isolated barchans over a distance of about 5km [*Jerolmack et al.*, 2012]. The second region begins approximately 7km downwind of the upwind margin, has dryer interdune surfaces outside of the capillary fringe (due to deepening of groundwater table), and is associated with both the gradual emergence of plants and a dramatic shift in the morphology of the dunes from barchan to parabolic [*Reitz et al.*, 2010; *Jerolmack et al.*, 2012; *Pelletier*, 2015]. There is a wide range of surface soil textures, including: dry, loose sand; dry, but highly compacted and cemented sand; wet sand and silt; and a range of surface crusts (Figure 4). These patterns make the dune field an ideal arid environment to study variations in soil erodibility and its environmental controls. First, the transition from wet interdunes to dry dune crests in the unvegetated region provides a gradient in soil moisture over a scale of less than 100 m. The effects of soil moisture on both the wind erosion threshold [*Neuman*, 2003; *Wiggs et al.*, 2004; *Ravi et al.*, 2006; *Edwards and Namikas*, 2009] and the resisting shear force [*Herminghaus*, 2005; *Richefeu et al.*, 2006] are well documented, and so provide a good test case for our new method. Second, the downwind decline in dune migration rate across the field is associated with an increasing gradient in biological activity — vegetation, and soil-stabilizing crusts [*Langston and Neuman*, 2005] — over a scale of kilometers. While it has been suggested that salt and biological crusts should inhibit soil erosion [*Belnap and Gillette*, 1998; *Langston and Neuman*, 2005], there are few systematic *in-situ* studies of the mechanical strength conferred to surface soils by different crust types. Shear strength tests were conducted at two transects to exploit the moisture and biological gradients (Figure 1A). Transect 1 was approximately 30m in length; it traversed an unvegetated barchan dune (Figure 1B) along its stoss side, from moist interdune to dry crest. Transect 1 was chosen in order to examine soil moisture control. We sampled eleven locations along transect 1 (Figure 5A), with intervals of approximately $1 \sim 3$m. Transect 2 occurred in the vegetated parabolic portion of the dunes (Figure 1C), approximately 5km downwind of Transect 1 and close to the downwind margin. Soil moisture variation is limited in this portion of the dune field due to the deeper groundwater table, and the primary spatial variation in surface soil characteristics is associated with a mosaic of biological and salt crusts. Transect 2 was thus chosen in order to sample the widest range of crusts. We sampled eleven different locations along transect 2 (Figure 5B), at intervals of $1 \sim 3$m on the stoss portion which was approximately 15m in length, and at intervals of $10 \sim 15$m on the interdune portion which was approximately 50m in length.

To characterize the spatial variation of erodibility *in-situ*, we mounted the direct-drive robotic leg on a mobile ground-based platform, the RHex robot [*Saranli et al.*, 2001a] (Figure 2A). RHex is a bio-inspired, hexapedal robot that exhibits high mobility over a variety of outdoor environments, including terrain with obstacles [*Saranli et al.*, 2001b], inclinations from hills [*Ilhan et al.*, 2018] and stairs [*Johnson et al.*, 2011], and desert dunes [*Qian et al.*, 2017; *Roberts et al.*, 2014a, b]. The RHex robot has been employed for various aeolian research expeditions [*Qian et al.*, 2017; *Roberts et al.*, 2014a, b; *Qian et al.*, 2016a; *Van Pelt et al.*, 2016; *Qian et al.*, 2016b], and has demonstrated its capability to perform a wide variety of measurements including wind speed, saltation grain counts, erodibility, in strong wind conditions to obtain high spatiotemporal resolution field datasets [*Qian et al.*, 2017]. For all shear experiments at White Sands, we used a 1.5cm-wide cylindric intruder. The shear depth was recorded by the robotic leg and used to calculate the normalized shear strength. To prevent variations in shear depth from test to test, we implemented a surface detection algorithm to allow the shear leg to gently touch down and detect the surface height before submerging to the desired shear depth of 5cm. For all field tests, the shear speed was set to $u = 1$cm/s to remain in the quasi-static regime [*Katsuragi and Durian*, 2007; *Goldman and Umbanhowar*, 2008; *Forterre and Pouliquen*, 2008], and the shear distance was set to 15cm to allow sufficient data range to calculate average shear strength. The shear direction was kept the same as the dominant wind-eroding direction (i.e., Northeast direction), which is also towards the largest gradient of the dune slope.

Soil moisture was characterized *in situ* using a volumetric water-content sensor (Decagon GS-1) that is based on the measurement of dielectric permittivity. Given known variations in water salinity at White Sands that might affect permittivity based moisture measurements, we also collected soil samples ($20 \sim 30$ml) from the same depth as the shear tests (≈ 5cm) to validate the moisture content. We determined water content in the laboratory using a chemical reaction, gas pressure-based moisture tester (Humboldt Speedy 2000). The Speedy test was chosen because of the difficulty involved in measuring moisture content in gypsum using classical gravimetric methods. When exposed to heat the mineralogic structure of gypsum changes as water disassociates from the mineral matrix. This leads to inaccurate moisture readings as interfacial water content is confounded with mineralogic water content. In contrast, the reagent used in the Humboldt Speedy tester, calcium carbide, reacts only to the interfacial water between grains, and therefore gives more accurate moisture measurements than most

alternative moisture measurement methods. The soil samples taken from the field were also analyzed to determine their grain-size distribution using an image-based method (Camsizer by Retsch), similar to the method described in [*Jerolmack et al.*, 2011].

2.1.2. Plowing laboratory experiment

To isolate the control of soil moisture on erodibility, we performed laboratory experiments in a 30cm long, 11cm wide sandbox with a controllable water-misting system (Figure 6A inset) that allows us to systematically vary soil moisture on the sand surface. We used coarse sand (Washed Play Sand, Home Depot, $D_{50} = 0.56$mm) as a model granular medium (grain size distribution see Figure 7); previous research [*Li et al.*, 2013] has demonstrated that bulk responses of granular media, despite variations in particle size and shape, are qualitatively similar. The water mister was mounted on a linear actuator (Figure 6A) that swept back and forth rapidly, essentially randomizing water droplet locations to provide an approximately spatially-uniform surface soil moisture. Before misting, beds of sand were prepared by pouring sand into the box and leveling the surface with a straight edge. We set the linear actuator travel length to 80cm and the travel speed to 5cm/s. After each misting cycle, we confirmed that the spatial distribution of soil moisture was approximately uniform by measuring at eight different locations using the Decagon moisture probe (Figure 6B). One limitation of the Decagon sensor (and most of other electrical property measurement based moisture probes) is that measurements of moisture are integrated over the depth of the probe — roughly 5cm — which is larger than the depth of the laboratory shear tests (2cm) and certainly wind-shear erosion tests (roughly a grain diameter; see below). Thus, we also measured surface-soil moisture using the Speedy moisture tester; for each test, one sample of six grams was scraped from as close to the soil surface as possible, in the center of the sandbox. The act of disturbing the surface introduced a degree of uncertainty into the measurement that was found to vary from $0 \sim 0.5\%$ moisture. Throughout the rest of the paper, moisture content is reported as percent wet weight, defined as $m_{water}/(m_{soil} + m_{water}) * 100[\%]$ where m is mass. Measurements from both the Decagon probe and Speedy tester were converted to water content using a custom calibration, by preparing different sand samples in the laboratory with known moisture content. To eliminate systematic error that might arise from granular material type, temperature and groundwater salinity, we also performed measurements on a completely dry bed; this provided an offset that was applied to the Decagon probe, based on the measurement from the Speedy tester. A separate calibration curve was also developed from the field data. The average soil moisture of the sandbox (Figure 6D) increased linearly with the number of misting cycles, indicating repeatable control.

After each misting cycle, we performed shear strength tests with the direct drive robotic leg (Figure 8A) in a manner similar to the field experiment. A total of 33 runs were performed with moisture increasing gradually from 0 to 20% (Figure 8B), which was approximately the saturation water content for our test granular media. Shear tests were performed following misting (Figure 8B), and actual soil moisture was then measured at three locations in the sandbox. For each number of misting cycles (*i.e.*, desired moisture content) we performed three repetitions of shear measurements (Figure 8B). We report all results of shear measurements with actual moisture measurements. The shear speed was set to the same value as field experiments (1cm/s); however, a larger cylindrical intruder with a diameter of 3.6cm was used, and the shear distance was set to 11cm to avoid boundary effects. We configured the cylinder to be horizontal (Figure 8A) to eliminate the force fluctuation due to the change in the end-effector orientation. In this study, all lab experiments were performed on a flat substrate, and therefore shear strength was isotropic in all shear directions. To compare lab and field results, soil shear resistance stress τ_r was calculated as average shear force normalized by the projected surface area of the intruder perpendicular to the shear direction, $W * d$, where W is the intruder width and d is the shear depth recorded by the robotic leg.

2.2. Vertical penetration measurements

In both laboratory and field plowing experiments, we obtained the measurements of granular resistance force in the vertical direction as the robotic leg penetrated into the soil (Figure 3C). At low intrusion speed, vertical resistance forces exerted on a intruder dragging in homogeneous granular media increase linearly with the penetration depth, the penetration resistance, and the projected surface area of the intruder[*Hill et al.*, 2005]. In our study, the intruder surface area was kept the same, and we characterize the soil penetration resistance using as the vertical penetration force per depth. For each measurement we performed a linear regression for vertical force *vs.* displacement for the entire intrusion range (shaded region in Figure 3D) to obtain the penetration resistance. Similar to the horizontal plowing experiments, the intrusion speed was kept low (1cm/s) to avoid grain inertia effects [*Katsuragi and Durian*, 2007; *Goldman and Umbanhowar*, 2008], ensuring that the measured penetration resistance force was friction dominated.

2.3. Yield stress "Kick-out" measurement in the laboratory

In the context of rheology, the plowing method above is a 'constant shear' experiment [*Gravish et al.*, 2010]. It is unclear, however, whether and how the resisting stress τ_r may be related to a more traditional yield stress. Yield stress describes the point at which a granular material loses rigidity and begins to flow [*Liu and Nagel*, 2010]. This behavior is not accessible in a constant shear experiment, where granular displacement is forced to occur. We thus designed a new "kick-out" test by measuring the threshold force to generate initial grain movement on a cylinder of 3.6cm by 1.2cm, attached through a 17.5cm lever arm (Figure 3E) to a direct-drive motor module (Ghost Robotics). We measure the yield stress based on the following principle: the cylindrical intruder attached to the level arm is subject to a controlled, slowly increasing motor torque ramp while displacement of the intruder and resisting force are carefully measured. At the torque associated with critical yield stress we expect the intruder to "kick out" of the granular medium, resulting in a jump in the resisting force followed by an associated displacement. Similar to the plowing test, the direct-drive motor used in this test does not have gear boxes so it responds sensitively to external torques and forces [*Kenneally et al.*, 2018]. This allowed for the resistive force of the sand in response to the applied torque of the motor to be measured. The resistive force is modelled as being normal to the surface area of the cylinder that is in contact with the sand bed. This force is converted into a stress by dividing by the effective surface area of the probe that is in contact with bed at the moment of failure.

The protocol for applying force to the sand bed and determining a shear strength was as follows. First, the probe tip was submerged 4 mm in diameter relative to the sand surface. The probe was positioned strictly normal to the sand at position $\pi/2$, defined by the reference frame pictured in

Figure 3F inset. A groove in the sand surface ensured that there were no compressive forces on the probe. This corresponds to the 'Time A' schematic in the subpanel of Figure 3F inset. After positioning, the force output of the motor was gradually increased. The sand deformed, though only slightly, in response to this force and the probe shifted off being strictly vertical by $0 \sim 0.1$ rad. Eventually, the force output reached a peak that represented the peak resistive force of the sand before failure. This can be seen in the 'Time B' schematic of Figure 3F inset. Next, a sudden failure of the sand bed occured and the probe 'kicked out' of its approximately vertical position. This can be seen in the 'Time C' schematic of Figure 3F inset. The peak resisting force can be converted to a peak stress, τ_p, which we take as a proxy for yield stress. This test was then repeated for different soil surface moistures ranging from $0 \sim 18\%$ percent, where the misting and bed preparation protocol was identical to the plowing tests. Because this was a destructive test of the sand surface, after each test a new, dry bed of sand was prepared and brought up to a given percent moisture within the range being tested. Measurements of soil moisture and kick-out tests were typically taken 10 to 15 minutes after misting; due to slow infiltation rate of water into the bed, it is possible that time-varying capillary pressures in the subsurface could exert some influence on surface soil strength that cannot be captured with surface soil moisture readings; we explore this effect in a later section.

In this study, the "kick-out" measurements was performed using a single motor, but we note that similar test can also be performed using the direct-drive robotic leg [*Kenneally et al.*, 2016] used in the plowing and penetration tests. Given that the derived quantity τ_p is a spatially-localized measure in an unconsolidated, low-cohesion soil under virtually no confinement, our definition of the yield stress is by necessity a working definition. We believe, however, that it captures the key dynamic; namely, the loss of rigidity of the area being probed. It is worth noting that the test developed here appears to work well for the pure, dry sand used in the study and also for more resistant, wet sand. This is not the case with traditional *in-situ* shear-vane testers that are often used to determine yield stress [*Dzuy and Boger*, 1985]; their sensitivity range limits them to soils with a significant clay content. The design of the motor for the current probe allows for very low magnitude, controlled forces to be applied to the surface, and read out from the motor at high resolution. Thus, small differences in the peak shear before failure can be reliably detected in the sandy soils used.

2.4. Threshold fluid-shear stress measurement in the laboratory

The final perturbation method for laboratory sands was to determine the critical fluid-shear stress necessary to initiate saltation, τ_c. The concept is that fluid shear stress is gradually ramped up until the moment significant transport is detected. Tests were undertaken using the Portable In Situ Wind Erosion Laboratory (PI-SWERL) descibed in [*Etyemezian et al.*, 2007], which uses a rotating annular ring enclosed in a chamber to generate wind shear close to the sand bed. Given the larger surface area required for the test, the PI-SWERL was placed in a larger sandbox with dimensions 1 x 1 x 0.15 m (Figure 3G). Tests thus involved a much larger volume of sand (and water) compared to the shear strength measurements above, and therefore it took more time to prepare beds of uniform soil moisture. On the other hand, the protocol for the PI-SWERL test resulted in much smaller disturbance to the sand surface compared to the other techniques. Accordingly, the same sand bed was used for multiple erosion tests, and was only replaced once visually obvious disturbance to the sand surface had occurred. The version of the PI-SWERL employed here was outfitted with two optical gate sensors near the annular shear ring. Peak voltages generated by the optical gate occur when saltating grains occlude the gate above a threshold area. Optical gate peak area is then obtained by integrating the area of observed optical peaks over 1 second. Shear stress was increased within the PI-SWERL by gradually increasing the rotation rate [RPM] of the annular shear ring, following the protocol shown in Figure 3H. Beyond a critical RPM (and associated wind shear stress), the optical gate peak area increases dramatically (Figure 3H); this is interpreted as the onset of sustained saltation. We chose an optical gate peak area of 5 [Vs] as the value associated with the critical RPM; a sensitivity analysis showed that results did not change significantly over a threshold range of $5 \sim 17$ [Vs]. The RPM associated with this threshold optical gate area was then converted to a critical shear stress τ_c using the empirical relation between RPM and fluid stress τ given in the PI-SWERL manual:

$$\tau = -4.051 \times 10^{-12} RPM^3 + 5.351 \times 10^{-8} RPM^2 - 2.201 \times 10^{-5} RPM + 0.0351. \quad (2)$$

It is important to note that τ_c estimated by the PI-SWERL may not be strictly analogous to an estimate resulting from a straight-line wind tunnel [*Sweeney et al.*, 2008], owing to the rotational nature of the shear and associated differences in turbulence structure, and limited development of a boundary layer due to the small chamber size. The shear stress values generated by the PI-SWERL, however, were sufficient to explore relative changes in the erosion threshold with soil moisture, and also to test for a relation between mechanical measures of shear resistance and the threshold fluid shear stress.

The misting procedure was the same as for the previous experiments, including a typical waiting period of 10 to 15 minutes between misting and measurement of soil moisture and shear resistance. Because the soil bed was re-used for several subsequent experiments, however, slow infiltration of water could potentially cause temporal drift in the subsurface moisture that cannot be detected with surface measurements, but that could influence capillary pressure and hence erosion resistance of surface soils. To test for such an effect, we conducted parallel tests with the PI-SWERL to determine τ_c as a function of soil moisture for two different infiltration times after misting; 5 to 10 minutes, and 90 minutes. Results indicate a distinct offset between the two waiting times, suggesting that developing subsurface moisture profiles exert some influence on surface erodibility that cannot be captured with surface-soil moisture measurements (Figure 9). This result reinforces the importance of waiting a consistent time between misting and taking measurements; all reported measurements for τ_c were conducted a maximum of fifteen minutes after the most recent misting cycle, in order to mitigate any secular drift effect.

3. Results

3.1. Spatial variation of soil erodibility in the field at White Sands

We first examine spatial changes in erodibility determined from our two field transects at White Sands (Figure 5A,D). The variables determined along each transect were the shear

strength measurements from the "plowing" test, and corresponding soil moisture using the Decagon probe.

The upwind "barchan transect" (Figure 5A) began in a modestly vegetated and visibly moist interdune, with soil moisture in the range of 4% $\sim$ 8% (Figure 5C). The transect followed the centerline of an unvegetated and actively migrating barchan dune, moving up the stoss side. Dune stoss sand was dryer than interdunes ($< 2\%$), but exhibited patches of visibly compacted and cemented sand (Figure 4E). The transect terminated at the barchan dune crest, where soil moisture remained comparable to the stoss side but sand was visibly loose and un-cemented. Measured shear strength values fluctuated, and increased slightly, moving from the moist interdune up to the mid-point of the dryer but compacted dune stoss. On approach to the dry and loose dune crest, however, shear strength dropped by roughly half to reach a minimum ($\approx 4.3 \pm 0.9$ N) at the crest (Figure 5B).

The downwind "parabolic transect" (Figure 5D) contained a mosaic of surface soil crusts (Figure 4D). The transect began in a heavily vegetated interdune close to the edge of a dune (location 0), where the soil surface was covered in a thin, tan-colored and potentially biological crust. The transect traversed several meters of interdune (locations 1-2; Figure 5D) that had a hard, white-salt surface crust before transitioning (location 3) onto the stoss face of a vegetated and stabilized parabolic dune. The stoss side was covered in patchy brown crusts that were likely calcium carbonate. Soil moisture was less than $\approx 1\%$ at all locations except the first two (locations 0 and 1; see Figure 5F). Despite the variety of surface crusts, shear strength varied little over the entire parabolic transect (Figure 5E). Although soil moisture was (for the most part) very low, shear strength in the parabolic transect was comparable to the wettest sands encountered in the barchan transect.

3.2. Comparison of soil erodibility dependence on moisture between field and laboratory measurements

At White Sands, the groundwater table is close to the surface, and therefore the barchan interdune soil surfaces are moist whereas the soil surface near the barchan crest is dry. We hypothesize that soil moisture effects dominate erodibility in the barchan dunes, while soil crusts act to strengthen soil in the parabolics. The influence of moisture on soil erodibility has been well characterized in the laboratory and field [*Chepil*, 1956; *Fecan et al.*, 1998]; these previous results provide a benchmark for testing our new shear-strength approach. In this study, we performed laboratory experiments to isolate the control of soil moisture on the measured shear strength of sand, using protocols discussed in Sec. 2.1.2. We found that shear strength increased rapidly as soil moisture increased from 0% to 3% (Figure 10). Beyond 3%, shear strength decreased as moisture content continued to increase (Figure 10). Measurements of soil strength at White Sands exhibited a similar non-monotonic dependence on moisture (Figure 10); however, there are discrepancies between laboratory and field data at higher soil moisture values. Field data exhibited overall higher strength in the higher moisture range ($> 5\%$) compared to laboratory measurements; these high-moisture locations correspond to interdune locations where crusts were also observed.

3.3. Soil response to mechanical and fluid perturbation methods

The above results suggest that the new robotic-shear device holds promise for reproducibly determining the mechanical strength of surface soils. As discussed above, however, it is not clear how shear strength from the "plowing" test is related to the wind erosion threshold or a mechanical yield strength. Moreover, granular physics studies have shown that bulk behavior of granular media depends sensitively on the perturbation methods [*Jaeger and Nagel*, 1992]. Accordingly, in this section we present results from three other tests conducted in the laboratory sandbox under varying soil moisture: a vertical penetration test, a yield-stress "kick out" test, and a wind erosion test.

The vertical penetration results were most similar to the "plowing" test (Figure 11B); penetration resistance was lowest for dry soil, increased rapidly to a maximum at 1% $\sim$ 2% where values plateaued, and decreased as moisture approached saturation. In contrast, peak stress from the "kick out" test increased approximately linearly with increasing moisture up to $\approx 7\%$, and then appeared to jump to a much higher value; the effective yield stress would likely continue to increase with higher moisture values, however we were unable to explore the moisture regime of $\approx 7\%$ to 17% due to the limited torque range of the motor. We were only able to recover a yield strength measurement again when soil moisture approached saturation (soil moisture $\approx 17\%$), and the yield stress dropped quickly to a value comparable to the dry case (Figure 11). The threshold wind stress determined from the PI-SWERL followed a similar trend to the kick-out yield strength; it increased roughly linearly up to a moisture of $\approx 7\%$. The maximum rotation rate of the PI-SWERL blade prohibited us from measuring beyond $\approx 7\%$, but the threshold wind stress likley would continue to increase with increasing soil moisture. Reported values of threshold wind stress for moisture values $> 7\%$ shown in (Figure 11) therefore represent minimum values. Unlike the yield stress measurements, however, threshold wind stress did not drop as the sand approached saturation.

4. Discussion

4.1. Environmental controls on shear strength at White Sands

The field measurements of shear strength (using the "plowing" test) and soil moisture at White Sands can begin to be understood by comparison to laboratory measurements, where soil moisture was changed systematically. For a range of soil moisture from 0 to 5%, shear strength values from the barchans and parabolics largely overlap with laboratory measurements showing a rapid increase with moisture followed by a gradual decline (Figure 10). Except for dry sand, however, field values for shear strength are in general larger than corresponding laboratory measurements (*e.g.*, 1.69N/cm^2 for field *vs.* 0.78 ± 0.04N/cm^2 for lab at 8 $\sim$ 10% moisture content; 1.31 ± 0.08N/cm^2 for field *vs.* 0.61 ± 0.12N/cm^2 for lab at 15 $\sim$ 20% moisture content). Thus, we conclude that soil moisture explains part, but not all, of the variation in shear strength of the White Sands surface soils. In the following paragraphs, we discuss additional environmental controls besides soil moisture that could play an important role on soil erodibility, and we discuss our future experiment plans to study these different factors by integrating our new method with improved techniques for measuring environmental variables.

One important environmental control is soil compaction. Considering the barchan dune transect, the wettest interdune sands had shear strengths that were twice as large as the dry and loose sand on the dune crest; this can be attributed mostly to the soil moisture effect. The relatively

dry sand on the dune stoss, however, had a strength similar to (and slightly larger than) the wet interdune sands. The dune stoss face is composed of gypsum sand that has been compacted and mildly cemented under deposition, and is now being exposed again by erosion due to dune migration [*McKee*, 1966]. It has been documented that compaction can influence the yield stress and rheology of granular materials [*Nedderman*, 1992; *Richard et al.*, 2005; *Gravish and Goldman*, 2014]. It is also likely that cementation — which is more common in White Sands than other dune fields due to the hygroscopic nature of gypsum [*Schenk and Fryberger*, 1988] — plays a role in strengthening the soil. Future laboratory experiments could and should tune granular compaction (e.g., *Gravish and Goldman* [2014]) to explicitly examine its effect on shear strength as measured with our robotic "plowing" test.

Another important environmental control is surface crust. Surface soils in the parabolic transect had low soil moisture values, for the most part. The sediments did not appear to be visibly compacted or cemented like the stoss side of the upwind barchan dune; yet their shear strength values were comparably large. We posit that the diverse surface crusts observed across the parabolic transect conferred strength to the surface soils. Others have noted that surface crusts may increase the resistance of desert surfaces to erosion [*Belnap and Gillette*, 1997, 1998]; our *in-situ* measurements of shear strength allow us to quantify this effect. At the few locations in the parabolic transect where soil moisture was high ($8\% \sim 16\%$), shear strengths were significantly larger than laboratory measurements at comparable soil moisture values (Figure 10). We speculated that the correlation of soil strength with soil moisture in these locations may result partly from other variables like crusting that co-vary with moisture. We observed that these locations corresponded to areas with higher levels of (apparently) biological crusts. Preliminary tests of shear strength at different vertical depths suggested that the biological crusts not only increased soil strength on the surface, but also strengthened the soil underneath the crust. This is likely due to chemical bonding that causes both crust development and grain aggregation[*Cerdà*, 1998; *Fattet et al.*, 2011]. This mechanism likely facilitates stabilization of the parabolic dunes at White Sands, since the overall erosion threshold was enhanced even when the surface crust was no longer intact. While the relationship between desert crusts and nearby vegetation is poorly understand, the fact that they usually occur together hints that the presence of certain types of crusts is necessary for healthy plant communities in some environments [*Belnap et al.*, 2001; *Lesica and Shelly*, 1992]. Our results show that one potential reason for this is that they make the surface harder to erode, helping plants to further establish a foothold in the soil. This lends further credence to the importance of desert crusts in maintaining the health of ecosystems in aeolian environments [*Collins et al.*, 2008]. In future field experiments, we plan to deploy the plowing method layer by layer with small shear depth (mm scale), to investigate the variation of soil erodibility in the vertical direction. Such investigation could provide insights on how surface crusts affect the erodibility of the soil underneath the crust.

Additional environmental controls such as grain size, or the repeated wetting-drying history of gypsum grains, could also affect soil erodibility. Exploring these controls, however, is currently beyond the scope of this paper and will be investigated in a future study. Furthermore, we note that future studies should address the effect of slope angle and shear direction. *Marvi et al.* [2014] suggested that shear resistance force decreased as slope inclination angle increased. This would indicate that our field data collected from the (sloping) stoss face may have slightly underestimated the actual strength of the soil.

4.2. Comparison of different mechanical tests for erodibility

For all probing techniques except the wind erosion test, a qualitatively similar and non-monotonic relation was observed between mechanical strength and soil moisture. This general behavior is consistent with previous studies on the mechanical strength of soil subject to varying degrees of saturation. For dry grains, the interparticle forces arise predominantly from friction. As pore spaces begin to fill with water, liquid capillary bridges form between grains that enhance the strength of the soil (think of sand castles). With the continuing addition of water, eventually the pore spaces become saturated and the strength of the soil drops [*Schubert*, 1975; *Kristensen et al.*, 1985; *Iveson et al.*, 2002; *Lu et al.*, 2007]. Considering the wind erosion test, it is not surprising that the threshold stress did not drop at saturation. In this case the surface likely becomes coated with a thin film of water, which would suppress direct entrainment by the wind and also damp collisions from saltating grains [*Barnocky and Davis*, 1988].

In terms of quantitative trends, the data from the four testing techniques break into two categories. Shear strength from the "plowing" test, and penetration resistance from the normal loading test, both showed a rapid rise in strength with increasing soil moisture that peaked at a low value of moisture, $\approx 1\%$ (Figure 10). This finding is consistent with the effective Coulomb cohesion that arises from capillary bridges in the so-called pendular state (discontinuous liquid phase), which increases nonlinearly with soil moisture and saturates at a few percent soil moisture [*Richefeu et al.*, 2006]. Strength measurements from both tests also exhibited a relatively rapid drop over the soil moisture range of 15% to 20%; i.e., approaching saturation. Results from the two tests differed for moisture values in between these two limits; shear strength declined continuously as soil moisture increased from 1% to 15%, while penetration resistance remained approximately constant. We do not yet understand the reason for the differences between these tests; however, the strength of wet granular materials is known to depend on the degree of confinement [*Richefeu et al.*, 2006].

Yield stress determined from the kick-out test, and the threshold fluid shear stress from the PI-SWERL, show similar trends to each other that are distinct from the other two methods discussed in the previous paragraph (Figure 11C). Both the yield stress and threshold fluid stress increase almost linearly with moisture until $\approx 5\%$. These trends are consistent with the increases in tensile strength reported experimentally by *Lu et al.* [2007] and *Schubert* [1975] for medium sand with a wide size distribution. This provides support that the increase in the strength of the sand comes from an increase in capillary pressure as the sand becomes more highly saturated. Moreover, the large rise in threshold fluid stress with moisture validates the observation of *Bisal and Hsieh* [1966] and *Wiggs et al.* [2004] that, under most conditions, soil above $4\% - 5\%$ moisture is difficult to erode by natural wind. Our observed linear trend is also consistent with the empirical results reported for τ_c of coarse sands of various wetness by *McKenna-Neuman and Nickling* [1989], although their reported trend only goes from $0\% - 2\%$ soil moisture. As mentioned, both the kick-out test and PI-SWERL data are suggestive of a jump in the yield stress as soil moisture increased from 5% to 7%, though our inability to measure yield stress at moisture values larger than 7%

(see above) makes this putative jump inconclusive. Others have reported an increase in mechanical yield strength at the transitional soil moisture zone between the pendular and funicular states in partially saturated soils [*Mitarai and Nori*, 2006].

Summing up our comparison of the four tests, each provides different and overlapping information on the mechanical strength of soil as tested by increasing soil moisture in a controlled laboratory setting. The kick-out test measure of yield strength was strongly correlated with fluid threshold stress, suggesting that a robotic kick-out test mounted on a robotic platform could be an effective and efficient tool for characterizing the susceptibility of soil to erosion by wind. A limitation of both tests is that yield strengths for soil moisture values $> 7\%$ could not be determined due to mechanical limitations. In practice, however, aeolian transport would be negligible for such soils because natural winds rarely get strong enough. Both the kick-out and PI-SWERL tests are explicitly designed to test yielding. It is not surprising that the plowing and penetration tests showed different behavior, as they are constant shear-rate tests that measure resistance below the yield point. These tests may not be good proxies for wind erosion, but they could be useful complementary measures for determining stability to plowing and trampling. At present we do not understand entirely the reasons for different trends among the four techniques; however, differences in confinement, the complex interaction of water and sand in partially-saturated soils, and shear-rate dependent rheology likely all play a role.

4.3. Challenges and open questions

Although we discussed our inability to determine threshold fluid stress with the PI-SWERL for $> 7\%$ soil moistures, we see that measurements begin to become unreliable at even lower values. In particular, once moisture values reach 5%, the variance in threshold fluid stress grows rapidly (Figure 11C). We speculate that this may be due to increasing variability in turbulent stresses in the PI-SWERL as the rotation rate gets larger; this degrades any estimate for τ_c that relies only on time-averaged flow velocities [*Diplas et al.*, 2008; *Durán et al.*, 2011; *Weaver and Wiggs*, 2011].

Another shortcoming of our laboratory approach relates to our considering soil strength as a function of soil moisture. Although soil moisture is easy to measure, it must be considered at best a proxy variable for pressures induced by the distribution of water in porous media. Capillary pressures, for example, arise from gradients in water content. This point is apparent in our tests of the influence of infiltration time on the observed trends in τ_c seen in Figure 9. For comparable soil moisture values, soil with a longer infiltration time was stronger. These results seem to support the idea proposed by *McKenna-Neuman and Nickling* [1989] that a soil's matric potential could be a more important control of τ_c than actual moisture content. In this work, surface soil moisture was chosen based on its feasbility for deployment on a robotic platform in the field, and also for comparison to other studies that usually report moisture rather than tension [*Bolte et al.*, 2011; *Wiggs et al.*, 2004]. Further work to establish whether or not the response of the mechanical yield strength test and measured τ_c remain consistent for different near-surface matric potentials is necessary.

It is an open question as to whether surface mechanical yield strength and τ_c respond similarly to other variables that control soil state. Compaction and cohesion are both known to influence yield strength and τ_c [*Meng et al.*, 2012; *Léonard and Richard*, 2004], but studies rarely if ever examine multiple measures of strength/erodibility. An interesting consideration is desert crusts, which are expected to create surface layers that are mechanically distinct from the subsurface. One may imagine a thin and smooth soil crust that is resistant to wind erosion, but that is easily pierced by a vertical penetration probe or a robotic shear leg. This raises the question more broadly of chacterizing erodibility in more stuctured or heterogeneous soils than the simple sands we have considered here. The force curves generated by our mechanical tests could become more complicated, and differences between normal and shear loading may arise that are indicative of anisotropy. If effects such as compaction and cohesion elicit different responses from the different mechanical tests, however, this may indicate that a suite of different tests could be used to disentangle the controls of these variables (and others, such as soil moisture). Future work should examine the control of these different parameters, in isolation and in concert.

Though further developments could extend the applicability of the proposed techniques to other settings (such as desert crusts or soils with significant organic matter), the existing data show that the technique could already be applied at some field sites where soil moisture is hypothesized to be the dominant control of variability in the threshold stress, such as most beaches [*Jackson and Nordstrom*, 1997]. Surface moisture is recognized as one of the primary control variables of τ_c in the field. However, the increase in τ_c associated with a given rise in moisture appears highly site dependent and difficult to model [*Webb and Strong*, 2011]. Rapid, direct estimates of τ_c provided by RHex or a similar robotic platform could overcome this problem. Given the rapidity with which the shear strength test can be performed, one practical way to field verify its ability to assess changes in sediment flux related to variation in τ_c would be to attempt to relate variations in measured sand flux to changes in surface shear strength in the spirit of *Wiggs et al.* [2004].

Improvements to the probe used in [*Qian et al.*, 2017] would enable the kick-out yield-strength test described here to be performed in conjunction with the constant displacement plowing test that has already shown potential in being able to characterize the erosive response of different substrates in the field. Figure 2A shows the design of a probe that is capable of performing both types of soil tests. Modifications to the probe tip to more directly engage the sand surface, rather than integrating the surface with several millimeters of sub-surface, are also under consideration. In future work, the direct-drive robotic shear leg will likely function as both locomotive limb and erodibility sensor — as opposed to being mounted on the robot body — increasing the versatility and usability of the system. We envision that increased availability of semi-autonomous force-feedback technology would allow field researchers to further improve the spatial resolution of soil erodibility measurements.

5. Conclusion

This study introduces a novel technique for assessing soil erodibility by a mobile robot bearing direct drive motors that manipulate the substrate while measuring forces and torques required to reach critical thresholds. The field test used the RHex robot as a platform to successfully gather data on erodibility across two different spatial gradients at White Sands, NM. Beyond demonstrating the feasibility of the method, the field and lab tests also allowed us to gather valuable information about how erodibility varies at White Sands dune field. The data collected during the field campaign highlight that the shear strength of natural desert soils

varies as a measurable consequence of soil moisture and surface crusts. We found that at the arid barchan dunes, soil erodibility increased from crest to the bottom of stoss, and then decreased as it entered the moist interdune area. Controlled lab tests indicated that the observed erodibility variation on barchans was largely dominated by soil moisture. On the vegetated parabolics, incased bio-activity and crust development played an important role in strengthening soil and stabilizing dune movement. This work demonstrates the potential of various mechanical tests performable by semi-autonomous robots to rapidly provide maps of a soil's susceptibility to mechanical perturbation and wind erosion over large areas.

Acknowledgments. We thank Sirui Ma, Sophie Bodek and Yosef Robele for help with instrumentation and experimentation. We thank Sonia Roberts, T.T.Topping, and Pramod Adhikari for help with field data collection. We thank Gavin Kenneally, and Avik De for their technical support on the development of the direct drive shear leg. We thank David Bustos for coordinating field work at White Sands. We thank White Sands National Park Services for their support in the field data collection. This research was supported by the National Science Foundation (NSF) under INSPIRE award, CISE NRI #1514882 and NRI INT award #1734355. All data used in the manuscript are publicly available on FigShare [*Qian et al.*, 2018a, b, c, d, e, f, g, h, i].

References

Albert, R., M. Pfeifer, A.-L. Barabási, and P. Schiffer (1999), Slow drag in a granular medium, *Physical review letters*, *82*(1), 205.

Asada, H., and K. Youcef-Toumi (1987), *Direct-drive robots: theory and practice*, MIT press.

Bakker, M. M., G. Govers, A. van Doorn, F. Quetier, D. Chouvardas, and M. Rounsevell (2008), The response of soil erosion and sediment export to land-use change in four areas of europe: the importance of landscape pattern, *Geomorphology*, *98*(3), 213–226.

Barnocky, G., and R. H. Davis (1988), Elastohydrodynamic collision and rebound of spheres: experimental verification, *The Physics of fluids*, *31*(6), 1324–1329.

Bekker, M. G. (1960), *Off-the-road locomotion: research and development in terramechanics*, University of Michigan Press.

Belnap, J., and D. A. Gillette (1997), Disturbance of biological soil crusts: impacts on potential wind erodibility of sandy desert soils in southeastern utah, *Land Degradation & Development*, *8*(4), 355–362.

Belnap, J., and D. A. Gillette (1998), Vulnerability of desert biological soil crusts to wind erosion: the influences of crust development, soil texture, and disturbance, *Journal of arid environments*, *39*(2), 133–142.

Belnap, J., R. Prasse, and K. Harper (2001), Influence of biological soil crusts on soil environments and vascular plants, in *Biological soil crusts: structure, function, and management*, pp. 281–300, Springer.

Bisal, F., and J. Hsieh (1966), Influence of moisture on erodibility of soil by wind., *Soil Science*, *102*(3), 143–146.

Bolte, K., P. Hartmann, H. Fleige, and R. Horn (2011), Determination of critical soil water content and matric potential for wind erosion, *Journal of soils and sediments*, *11*(2), 209–220.

Breshears, D. D., J. J. Whicker, C. B. Zou, J. P. Field, and C. D. Allen (2009), A conceptual framework for dryland aeolian sediment transport along the grassland–forest continuum: effects of woody plant canopy cover and disturbance, *Geomorphology*, *105*(1), 28–38.

Celik, I. (2005), Land-use effects on organic matter and physical properties of soil in a southern mediterranean highland of turkey, *Soil and Tillage Research*, *83*(2), 270–277.

Cerdà, A. (1998), Soil aggregate stability under different mediterranean vegetation types, *Catena*, *32*(2), 73–86.

Chepil, W. (1956), Influence of moisture on erodibility of soil by wind1, *Soil Science Society of America Journal*, *20*(2), 288–292.

Chepil, W., and N. Woodruff (1963), The physics of wind erosion and its control1, in *Advances in agronomy*, vol. 15, pp. 211–302, Elsevier.

Cho, G.-C., J. Dodds, and J. C. Santamarina (2006), Particle shape effects on packing density, stiffness, and strength: natural and crushed sands, *Journal of geotechnical and geoenvironmental engineering*, *132*(5), 591–602.

Collins, S. L., R. L. Sinsabaugh, C. Crenshaw, L. Green, A. Porras-Alfaro, M. Stursova, and L. H. Zeglin (2008), Pulse dynamics and microbial processes in aridland ecosystems, *Journal of Ecology*, *96*(3), 413–420.

Cosentino, D., C. Chenu, and Y. Le Bissonnais (2006), Aggregate stability and microbial community dynamics under drying–wetting cycles in a silt loam soil, *Soil Biology and Biochemistry*, *38*(8), 2053–2062.

Dai, A. (2013), Increasing drought under global warming in observations and models, *Nature Climate Change*, *3*(1), 52–58.

Diplas, P., C. L. Dancey, A. O. Celik, M. Valyrakis, K. Greer, and T. Akar (2008), The role of impulse on the initiation of particle movement under turbulent flow conditions., *Science (New York, N.Y.)*, *322*(5902), 717–20, doi:10.1126/science.1158954.

Dregne, H. E., and N.-T. Chou (1992), Global desertification dimensions and costs, *Degradation and restoration of arid lands*, pp. 73–92.

Durán, O., P. Claudin, and B. Andreotti (2011), On aeolian transport: Grain-scale interactions, dynamical mechanisms and scaling laws, *Aeolian Research*, *3*(3), 243–270.

Dzuy, N. Q., and D. Boger (1985), Direct yield stress measurement with the vane method, *Journal of rheology*, *29*(3), 335–347.

Edwards, B. L., and S. L. Namikas (2009), Small-scale variability in surface moisture on a fine-grained beach: implications for modeling aeolian transport, *Earth Surface Processes and Landforms*, *34*(10), 1333–1338.

Etyemezian, V., G. Nikolich, S. Ahonen, M. Pitchford, M. Sweeney, R. Purcell, J. Gillies, and H. Kuhns (2007), The portable in situ wind erosion laboratory (pi-swerl): A new method to measure pm 10 windblown dust properties and potential for emissions, *Atmospheric Environment*, *41*(18), 3789–3796.

Fattet, M., Y. Fu, M. Ghestem, W. Ma, M. Foulonneau, J. Nespoulous, Y. Le Bissonnais, and A. Stokes (2011), Effects of vegetation type on soil resistance to erosion: Relationship between aggregate stability and shear strength, *Catena*, *87*(1), 60–69.

Fecan, F., B. Marticorena, and G. Bergametti (1998), Parametrization of the increase of the aeolian erosion threshold wind friction velocity due to soil moisture for arid and semi-arid areas, in *Annales Geophysicae*, vol. 17, pp. 149–157, Springer.

Forterre, Y., and O. Pouliquen (2008), Flows of dense granular media, *Annu. Rev. Fluid Mech.*, *40*, 1–24.

Fredlund, D. G., A. Xing, M. D. Fredlund, and S. Barbour (1996), The relationship of the unsaturated soil shear to the soil-water characteristic curve, *Canadian Geotechnical Journal*, *33*(3), 440–448.

Gillette, D. (1978), Tests with a portable wind tunnel for determining wind erosion threshold velocities, *Atmospheric Environment (1967)*, *12*(12), 2309–2313.

Gillette, D. A., J. Adams, A. Endo, D. Smith, and R. Kihl (1980), Threshold velocities for input of soil particles into the air by desert soils, *Journal of Geophysical Research: Oceans*, *85*(C10), 5621–5630.

Giovannini, G., R. Vallejo, S. Lucchesi, S. Bautista, S. Ciompi, and J. Llovet (2001), Effects of land use and eventual fire on soil erodibility in dry mediterranean conditions, *Forest Ecology and Management*, *147*(1), 15–23.

Goldman, D. I., and P. Umbanhowar (2008), Scaling and dynamics of sphere and disk impact into granular media, *Physical Review E*, *77*(2), 021,308.

Goossens, D., and B. Buck (2009), Dust dynamics in off-road vehicle trails: measurements on 16 arid soil types, nevada, usa, *Journal of Environmental Management*, *90*(11), 3458–3469.

Goudie, A., and N. Middleton (2001), Saharan dust storms: nature and consequences, *Earth-Science Reviews*, *56*(1), 179–204.

Gravish, N., and D. I. Goldman (2014), Effect of volume fraction on granular avalanche dynamics, *Physical Review E*, *90*(3), 032,202.

Gravish, N., P. B. Umbanhowar, and D. I. Goldman (2010), Force and flow transition in plowed granular media, *Physical review letters*, *105*(12), 128,301.

Herminghaus, S. (2005), Dynamics of wet granular matter, *Advances in Physics*, *54*(3), 221–261.

Hill, G., S. Yeung, and S. Koehler (2005), Scaling vertical drag forces in granular media, *EPL (Europhysics Letters)*, *72*(1), 137.

Howell, D., R. Behringer, and C. Veje (1999), Stress fluctuations in a 2d granular couette experiment: a continuous transition, *Physical Review Letters*, *82*(26), 5241.

Ilhan, B. D., A. M. Johnson, and D. E. Koditschek (2018), Autonomous legged hill ascent, *Journal of Field Robotics*.

Iveson, S. M., J. A. Beathe, and N. W. Page (2002), The dynamic strength of partially saturated powder compacts: the effect of liquid properties, *Powder Technology*, *127*(2), 149–161.

Jackson, N. L., and K. F. Nordstrom (1997), Effects of time-dependent moisture content of surface sediments on aeolian transport rates across a beach, wildwood, new jersey, usa, *Earth Surface Processes and Landforms*, *22*(7), 611–621.

Jaeger, H. M., and S. R. Nagel (1992), Physics of the granular state, *Science*, *255*(5051), 1523–1531.

Jerolmack, D. J., M. D. Reitz, and R. L. Martin (2011), Sorting out abrasion in a gypsum dune field, *Journal of Geophysical Research: Earth Surface*, *116*(F2).

Jerolmack, D. J., R. C. Ewing, F. Falcini, R. L. Martin, C. Masteller, C. Phillips, M. D. Reitz, and I. Buynevich (2012), Internal boundary layer model for the evolution of desert dune fields, *Nature Geoscience*, *5*(3), 206–209.

Johnson, A. M., M. T. Hale, G. Haynes, and D. E. Koditschek (2011), Autonomous legged hill and stairwell ascent, in *Safety, Security, and Rescue Robotics (SSRR), 2011 IEEE International Symposium on*, pp. 134–142, IEEE.

Katsuragi, H., and D. J. Durian (2007), Unified force law for granular impact cratering, *Nature Physics*, *3*(6), 420–423.

Kenneally, G., and D. E. Koditschek (2015), Leg design for energy management in an electromechanical robot, in *IEEE/RSJ International Conference on Intelligent Robots and Systems*.

Kenneally, G., A. De, and D. E. Koditschek (2016), Design principles for a family of direct-drive legged robots, *IEEE Robotics and Automation Letters*, *1*(2), 900–907.

Kenneally, G., W.-H. Chen, and D. E. Koditschek (2018), Actuator transparency and the energetic cost of proprioception, in *Proc. Int. Symp. Exp Rob.*, p. (to appear), IFRR.

Kocurek, G., and R. C. Ewing (2005), Aeolian dune field self-organization–implications for the formation of simple versus complex dune-field patterns, *Geomorphology*, *72*(1), 94–105.

Kocurek, G., M. Carr, R. Ewing, K. G. Havholm, Y. Nagar, and A. Singhvi (2007), White sands dune field, new mexico: age, dune dynamics and recent accumulations, *Sedimentary Geology*, *197*(3), 313–331.

Kok, J. F., E. J. Parteli, T. I. Michaels, and D. B. Karam (2012), The physics of wind-blown sand and dust, *Reports on progress in Physics*, *75*(10), 106,901.

Kristensen, H., P. Holm, and T. Schaefer (1985), Mechanical properties of moist agglomerates in relation to granulation mechanisms part i. deformability of moist, densified agglomerates, *Powder Technology*, *44*(3), 227–237.

Kutiel, P., H. Zhevelev, and R. Harrison (1999), The effect of recreational impacts on soil and vegetation of stabilised coastal dunes in the sharon park, israel, *Ocean & Coastal Management*, *42*(12), 1041–1060.

Langford, R. P. (2003), The holocene history of the white sands dune field and influences on eolian deflation and playa lakes, *Quaternary International*, *104*(1), 31–39.

Langston, G., and C. M. Neuman (2005), An experimental study on the susceptibility of crusted surfaces to wind erosion: a comparison of the strength properties of biotic and salt crusts, *Geomorphology*, *72*(1-4), 40–53.

Léonard, J., and G. Richard (2004), Estimation of runoff critical shear stress for soil erosion from soil shear strength, *Catena*, *57*(3), 233–249.

Lesica, P., and J. S. Shelly (1992), Effects of cryptogamic soil crust on the population dynamics of arabis fecunda (brassicaceae), *American Midland Naturalist*, pp. 53–60.

Li, C., T. Zhang, and D. I. Goldman (2013), A terradynamics of legged locomotion on granular media, *science*, *339*(6126), 1408–1412.

Li, X., F. Tian, R. Jia, Z. Zhang, and L. Liu (2010), Do biological soil crusts determine vegetation changes in sandy deserts? implications for managing artificial vegetation, *Hydrological Processes*, *24*(25), 3621–3630.

Li, X.-R., X.-P. Wang, T. Li, and J.-G. Zhang (2002), Microbiotic soil crust and its effect on vegetation and habitat on artificially stabilized desert dunes in tengger desert, north china, *Biology and Fertility of Soils*, *35*(3), 147–154.

Liddle, M., and P. Grieg-Smith (1975), A survey of tracks and paths in a sand dune ecosystem. ii. vegetation, *Journal of Applied Ecology*, pp. 909–930.

Liu, A. J., and S. R. Nagel (2010), The jamming transition and the marginally jammed solid, *Annu. Rev. Condens. Matter Phys.*, *1*(1), 347–369.

Loye-Pilot, M., J. Martin, and J. Morelli (1986), Influence of saharan dust on the rain acidity and atmospheric input to the mediterranean, *Nature*, *321*(6068), 427–428.

Lu, N., B. Wu, and C. P. Tan (2007), Tensile strength characteristics of unsaturated sands, *Journal of Geotechnical and Geoenvironmental Engineering*, *133*(2), 144–154.

Majmudar, T. S., and R. P. Behringer (2005), Contact force measurements and stress-induced anisotropy in granular materials, *Nature*, *435*(7045), 1079.

Martin, R. L., and J. F. Kok (2017), Wind-invariant saltation heights imply linear scaling of aeolian saltation flux with shear stress, *Science advances*, *3*(6), e1602,569.

Marvi, H., C. Gong, N. Gravish, H. Astley, M. Travers, R. L. Hatton, J. R. Mendelson, H. Choset, D. L. Hu, and D. I. Goldman (2014), Sidewinding with minimal slip: Snake and robot ascent of sandy slopes, *Science*, *346*(6206), 224–229.

McKee, E. D. (1966), Structures of dunes at white sands national monument, new mexico (and a comparison with structures of dunes from other selected areas) 1, *Sedimentology*, *7*(1), 3–69.

McKenna-Neuman, C., and W. Nickling (1989), A theoretical and wind tunnel investigation of the effect of capillary water on the entrainment of sediment by wind, *Canadian Journal of Soil Science*, *69*(1), 79–96.

Meng, X.-m., Y.-g. Jia, H.-x. Shan, Z.-n. Yang, and J.-w. Zheng (2012), An experimental study on erodibility of intertidal sediments in the yellow river delta, *International Journal of Sediment Research*, *27*(2), 240–249.

Mitarai, N., and F. Nori (2006), Wet granular materials, *Advances in Physics*, *55*(1-2), 1–45.

Nedderman, R. (1992), Statics and kinematics of granular flows.

Neuman, C. M. (2003), Effects of temperature and humidity upon the entrainment of sedimentary particles by wind, *Boundary-Layer Meteorology*, *108*(1), 61–89.

Pelletier, J. D. (2015), Controls on the large-scale spatial variations of dune field properties in the barchanoid portion of white sands dune field, new mexico, *Journal of Geophysical Research: Earth Surface*, *120*(3), 453–473.

Qian, F., N. Lancaster, G. Nikolich, D. J. Jerolmack, S. F. Roberts, P. Reverdy, S. R. Van Pelt, T. M. Zobeck, T. Shipley, P. Adhikari, and D. E. Koditschek (2016a), Measurement of aeolian processes with a robotic platform, in *GSA Annual Meeting*.

Qian, F., D. B. Lee, S. Ma, D. E. Koditschek, and D. J. Jerolmack (2016b), Characterization of soil erodibility through mechanical shear measurements, in *AGU Fall Meeting*.

Qian, F., D. Jerolmack, N. Lancaster, G. Nikolich, P. Reverdy, S. Roberts, T. Shipley, R. S. Van Pelt, T. M. Zobeck, and D. E. Koditschek (2017), Ground robotic measurement of aeolian processes, *Aeolian Research*, *27*, 1–11.

Qian, F., D. Lee, G. Nikolich, D. Koditschek, and D. Jerolmack (2018a), Shear strength data (WhiteSands - barchan), doi: 10.6084/m9.figshare.7056350.v2.

Qian, F., D. Lee, G. Nikolich, D. Koditschek, and D. Jerolmack (2018b), Shear strength data (WhiteSands - parabolics), doi: 10.6084/m9.figshare.7056353.v2.

Qian, F., D. Lee, G. Nikolich, D. Koditschek, and D. Jerolmack (2018c), Shear strength data (laboratory), doi: 10.6084/m9.figshare.7056380.v2.

Qian, F., D. Lee, G. Nikolich, D. Koditschek, and D. Jerolmack (2018d), scripts to process shear strength data, doi: 10.6084/m9.figshare.7056413.v2.

Qian, F., D. Lee, G. Nikolich, D. Koditschek, and D. Jerolmack (2018e), processed shear strength data (field and lab), doi: 10.6084/m9.figshare.7056389.v2.

Qian, F., D. Lee, G. Nikolich, D. Koditschek, and D. Jerolmack (2018f), kick out experiment data, doi: 10.6084/m9.figshare.7056425.v2.

Qian, F., D. Lee, G. Nikolich, D. Koditschek, and D. Jerolmack (2018g), piswerl experiment data, doi: 10.6084/m9.figshare.7056434.v2.

Qian, F., D. Lee, G. Nikolich, D. Koditschek, and D. Jerolmack (2018h), scripts for kick-out and PiSwerl experiment control and analysis, doi:10.6084/m9.figshare.7056443.v3.

Qian, F., D. Lee, G. Nikolich, D. Koditschek, and D. Jerolmack (2018i), processed data for kick-out and PiSwerl experiments, doi:10.6084/m9.figshare.7056449.v3.

Ravi, S., T. M. Zobeck, T. M. Over, G. S. Okin, and P. D'ODORICO (2006), On the effect of moisture bonding forces in air-dry soils on threshold friction velocity of wind erosion, *Sedimentology*, *53*(3), 597–609.

Reich, P., S. Numbem, R. Almaraz, and H. Eswaran (2001), Land resource stresses and desertification in africa, *Agro-Science*, *2*(2).

Reitz, M. D., D. J. Jerolmack, R. C. Ewing, and R. L. Martin (2010), Barchan-parabolic dune pattern transition from vegetation stability threshold, *Geophysical Research Letters*, *37*(19).

Richard, P., M. Nicodemi, R. Delannay, P. Ribiere, and D. Bideau (2005), Slow relaxation and compaction of granular systems, *Nature materials*, *4*(2), 121–128.

Richefeu, V., M. S. El Youssoufi, and F. Radjai (2006), Shear strength properties of wet granular materials, *Physical Review E*, *73*(5), 051,304.

Roberts, S., J. Duperret, A. M. Johnson, S. van Pelt, T. Zobeck, N. Lancaster, and D. E. Koditschek (2014a), Desert rhex technical report: Jornada and white sands trip, in *University of Pennsylvania Technical Report*.

Roberts, S. F., J. M. Duperret, X. Li, H. Wang, and D. Koditschek (2014b), Desert rhex technical report: Tengger desert trip, in *University of Pennsylvania Technical Report*.

Rosenfeld, D., Y. Rudich, and R. Lahav (2001), Desert dust suppressing precipitation: A possible desertification feedback loop, *Proceedings of the National Academy of Sciences*, *98*(11), 5975–5980.

Santamarina, J., and G.-C. Cho (2004), Soil behaviour: The role of particle shape, in *Advances in geotechnical engineering: The skempton conference*, vol. 1, pp. 604–617, Citeseer.

Saranli, U., M. Buehler, and D. E. Koditschek (2001a), Rhex: A simple and highly mobile hexapod robot, *The International Journal of Robotics Research*, *20*(7), 616–631.

Saranli, U., M. Buehler, and D. E. Koditschek (2001b), Rhex: A simple and highly mobile hexapod robot, *The International Journal of Robotics Research*, *20*(7), 616–631.

Schenk, C. J., and S. G. Fryberger (1988), Early diagenesis of eolian dune and interdune sands at white sands, new mexico, *Sedimentary Geology*, *55*(1-2), 109–120.

Schlesinger, W. H., J. F. Reynolds, G. L. Cunningham, L. F. Huenneke, W. M. Jarrell, R. A. Virginia, W. G. Whitford, et al. (1990), Biological feedbacks in global desertification., *Science(Washington)*, *247*(4946), 1043–1048.

Schubert, H. (1975), Tensile strength of agglomerates, *Powder Technology*, *11*(2), 107–119.

Shao, Y., M. Raupach, and P. Findlater (1993), Effect of saltation bombardment on the entrainment of dust by wind, *Journal of Geophysical Research: Atmospheres*, *98*(D7), 12,719–12,726.

Sweeney, M., V. Etyemezian, T. Macpherson, W. Nickling, J. Gillies, G. Nikolich, and E. McDonald (2008), Comparison of pi-swerl with dust emission measurements from a straight-line field wind tunnel, *Journal of Geophysical Research: Earth Surface*, *113*(F1).

Trimble, S. W., and A. C. Mendel (1995), The cow as a geomorphic agenta critical review, *Geomorphology*, *13*(1-4), 233–253.

Van Oost, K., G. Govers, S. De Alba, and T. Quine (2006), Tillage erosion: a review of controlling factors and implications for soil quality, *Progress in Physical Geography*, *30*(4), 443–466.

Van Pelt, S., T. Zobeck, T. Kandakji, J. Strack, D. E. Koditschek, S. F. Roberts, and P. Reverdy (2016), Mobile characterization of wind flow fields around solid and porous objects, in *AGU Fall Meeting*.

Weaver, C. M., and G. F. Wiggs (2011), Field measurements of mean and turbulent airflow over a barchan sand dune, *Geomorphology*, *128*(1-2), 32–41.

Webb, N. P., and C. L. Strong (2011), Soil erodibility dynamics and its representation for wind erosion and dust emission models, *Aeolian Research*, *3*(2), 165–179.

Webb, R. H. (1983), Compaction of desert soils by off-road vehicles, in *Environmental effects of off-road vehicles*, pp. 51–79, Springer.

Webb, R. H., and H. G. Wilshire (2012), *Environmental effects of off-road vehicles: impacts and management in arid regions*, Springer Science & Business Media.

Wiggs, G., A. Baird, and R. Atherton (2004), The dynamic effects of moisture on the entrainment and transport of sand by wind, *Geomorphology*, *59*(1-4), 13–30.

Wolfe, S., and W. Nickling (1996), Shear stress partitioning in sparsely vegetated desert canopies, *Earth Surface Processes and Landforms*, *21*(7), 607–619.

Wong, J., et al. (1989), Terramechanics and off-road vehicles., *Terramechanics and off-road vehicles.*

Wu, B., and L. J. Ci (2002), Landscape change and desertification development in the mu us sandland, northern china, *Journal of Arid Environments*, *50*(3), 429–444.

Yang, D., S. Kanae, T. Oki, T. Koike, and K. Musiake (2003), Global potential soil erosion with reference to land use and climate changes, *Hydrological processes*, *17*(14), 2913–2928.

Yong-Zhong, S., L. Yu-Lin, C. Jian-Yuan, and Z. Wen-Zhi (2005), Influences of continuous grazing and livestock exclusion on soil properties in a degraded sandy grassland, inner mongolia, northern china, *Catena*, *59*(3), 267–278.

Zender, C. S., D. Newman, and O. Torres (2003), Spatial heterogeneity in aeolian erodibility: Uniform, topographic, geomorphic, and hydrologic hypotheses, *Journal of Geophysical Research: Atmospheres*, *108*(D17).

Corresponding author: Douglas J. Jerolmack, Department of Earth and Environmental Science, University of Pennsylvania, Philadelphia, PA, USA. (sediment@sas.upenn.edu)

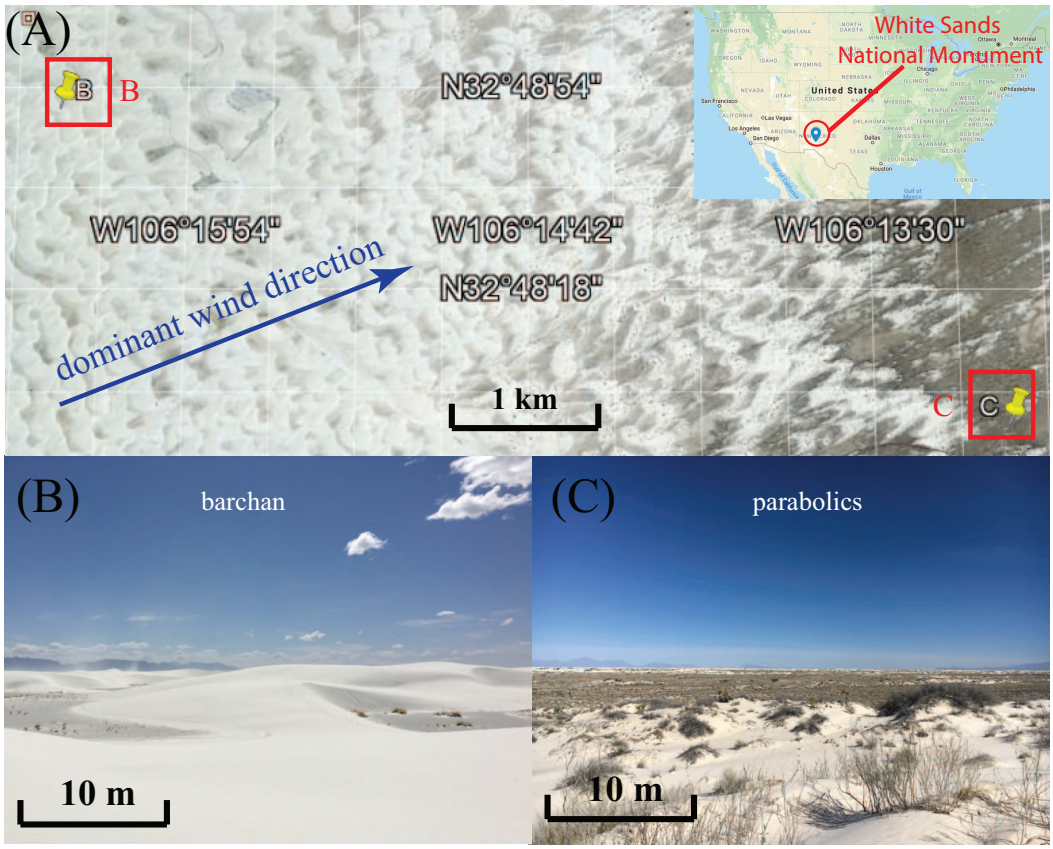

Figure 1. White Sands National Monument, NM, a Southwestern desert in the United States. (A) Google Maps image of White Sands. Black arrow indicates direction of the dominant wind, and associated dune migration. Red squares indicate the locations of barchan (square B) and parabolic (square C) dunes where field measurements in this paper were conducted. Inset shows the location of the White Sands National Monument on the US map. (B) Photo of barchan dunes. (C) Photo of parabolic dunes.

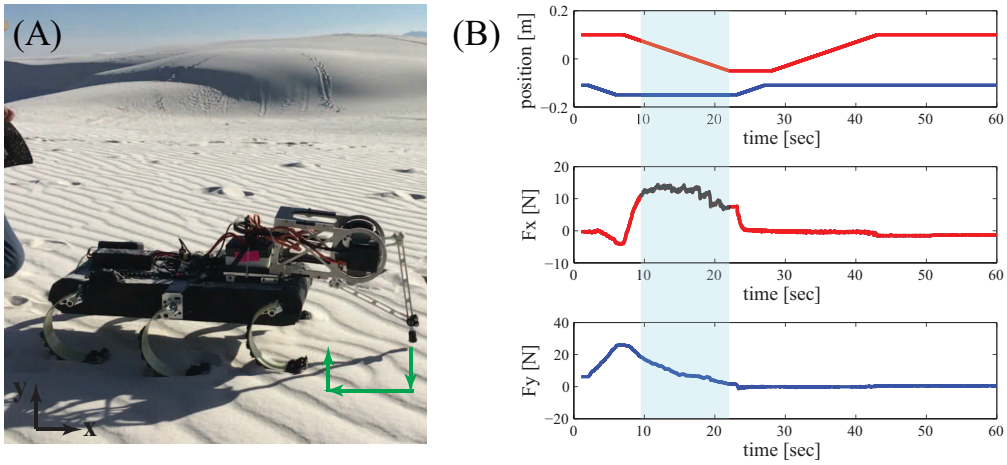

Figure 2. Robotic shear strength measurements for soil erodibility characterization. (A) Field experiment setup. The RHex robot[*Saranli et al.*, 2001a] walks in the dune field at White Sands National Monument, NM, stops at desired locations and performs mechanical shear test at the desired shear depth using a direct-drive leg mounted on its back. Green arrows indicate the moving trajectory of the robot leg end-effector during a complete plowing test, including vertical insertion, horizontal shear, and withdrawal. (B) A sample set of measurements from our field data. In the first row of the plots, the red and blue curves represent the recorded horizontal (x) and vertical (y) positions, respectively, of the end effector relative to the center of motors. In the second and third rows, the red and blue curves represent the horizontal force (F_x) and vertical force (F_y) exerted on the end effector, respectively. We characterize the shear strength as the average shear resistance force ($\bar{F}_x$) during the steady state range of the shear motion (shaded region).

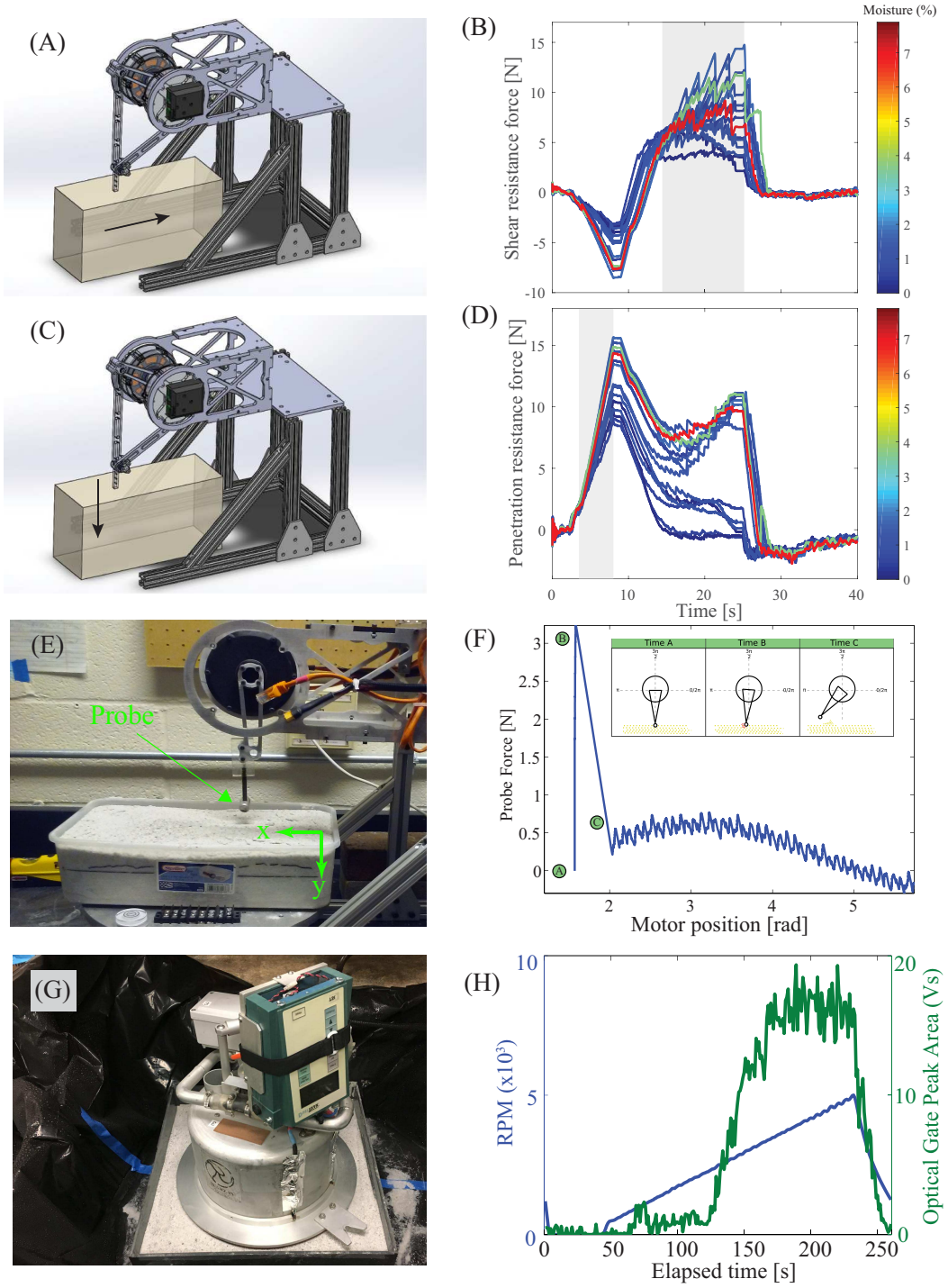

Figure 3. Perturbation methods and soil responses. (A) Horizontal shear experiment setup. (B) Shear resistance force responses obtained from the plowing method shown in (A) from White Sands. Color represents moisture content. Shaded region represents the shear duration. (C) Vertical intrusion experiment setup. (D) Penetration resistance force responses obtained from the vertical intrusion method shown in (C) from White Sands. Color represents moisture content. Shaded region represents the intrusion duration. (E) Kick-out experiment setup. (F) Yield force responses obtained from the kick-out method shown in (E). (G) PI-SWERL experiment setup. (H) Fan RPM and resulting saltated sediment counts measured by the optical gate sensor from the PI-SWERL experiment shown in (G).

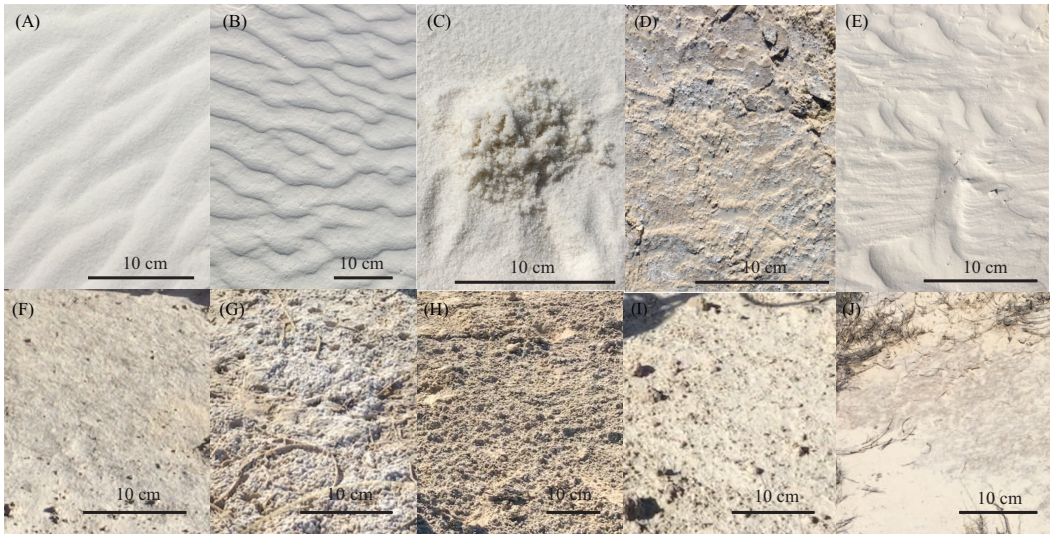

Figure 4. Variety of soil surfaces at White Sands. (A) Dry, loosely packed gypsum sand at the crest of a barchan dune. (B) Dry, closely packed gypsum sand on a barchan stoss. (C) Moist gypsum sand from 1 $\sim$ 2cm subsurface on a barchan dune. (D) Crusted soil surface found in the interdune area. (E) Cemented gypsum sand at the beginning of a barchan stoss. (F) Thin-crusted soil surface found in a parabolic interdune. (G) Hard, white crust found in a parabolic interdune. (H) Dark brown crust found in the parabolic interdune. (I) Thin, beige crusted soil found near the toe of a parabolic. (J) Patchy brown crusts found on parabolic stoss.

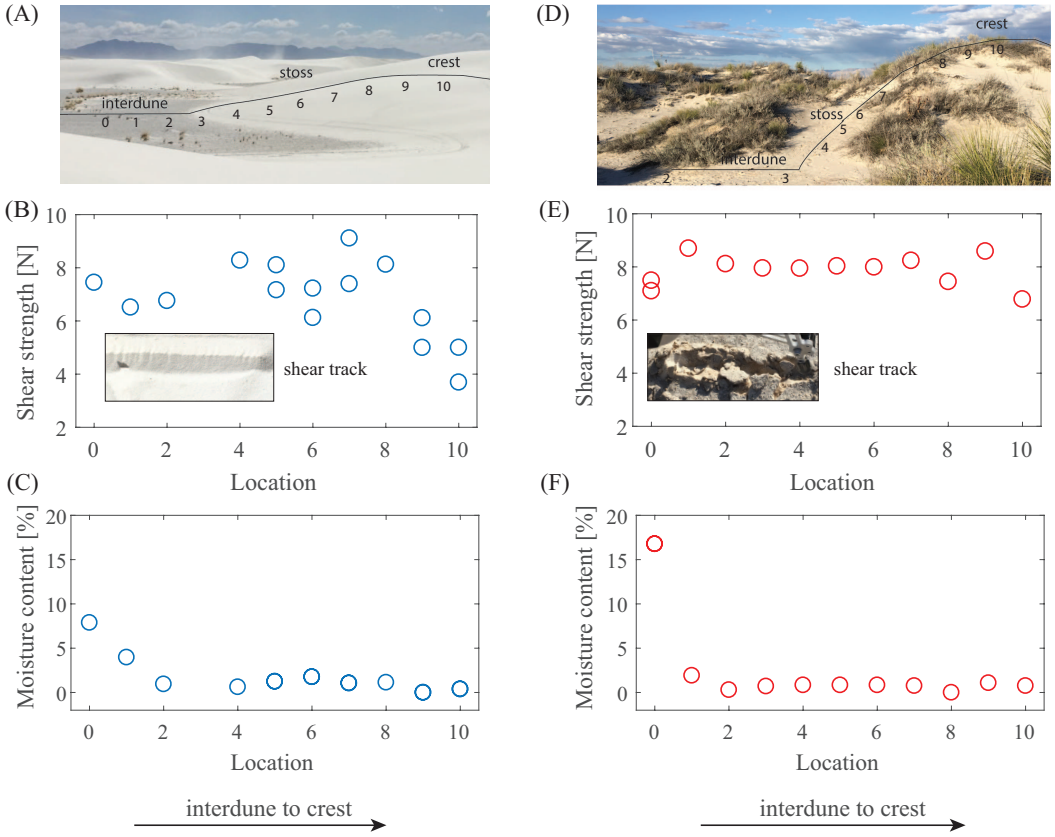

Figure 5. Spatial variation of soil shear strength measured from barchan and parabolic dunes at White Sands National Monument. (A) Distribution of locations on a barchan dune where shear strength data were collected. (B) Average shear resistance force measured by the direct-drive robotic leg from interdune to the dune crest at an arid barchan dune. Inset: track left on the soil surface after the shear test. (C) Moisture content measured on the barchan transect. (D) Distribution of locations on a parabolic dunes where shear strength data were collected. Due to the large area sampled in the parabolic interdune, location 0 and 1 were farther away (> 10m) from the toe of stoss and therefore not within the scale captured by the photo. (E) Average shear resistance force measured by the direct-drive robotic leg from interdune to the dune crest at a vegetated, parabolic dune. Inset: track left on the crusted soil surface after the shear test. (F) Moisture content measured on the parabolics transect.

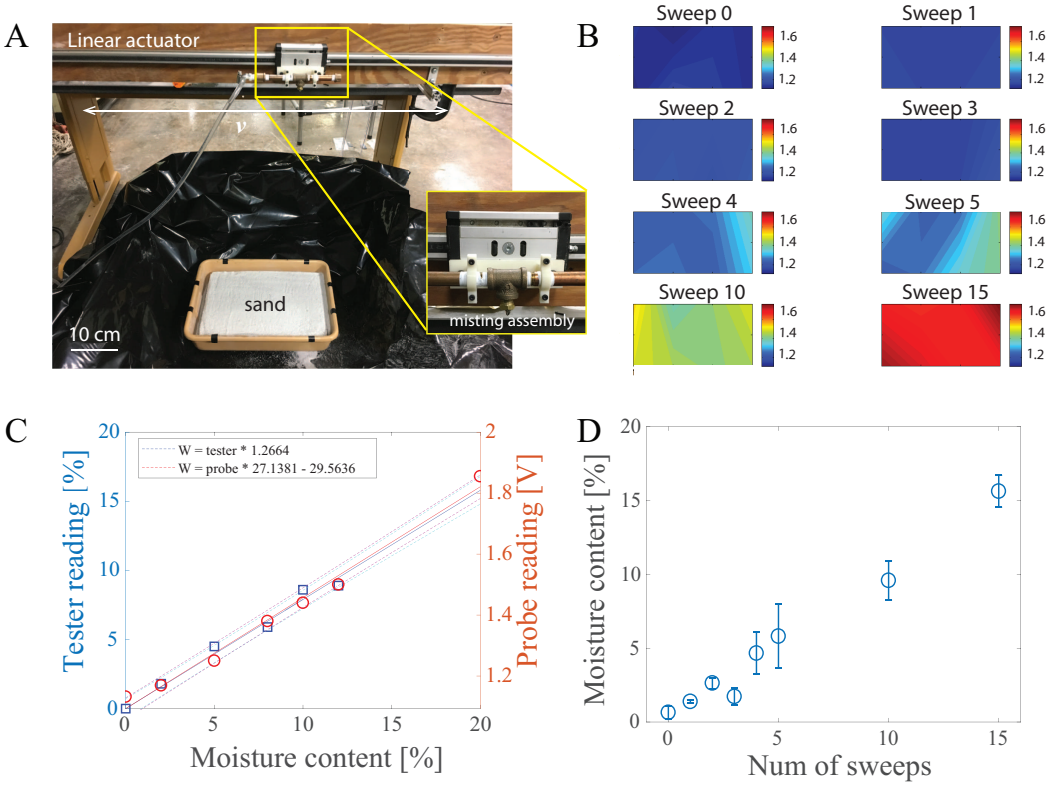

Figure 6. Moisture control and measurement. (A) Moisture control setup. A mister assembly was mounted on a linear actuator that swept back and forth to evenly wet the sand. (B) Soil moisture distribution in the sandbox after various number of misting cycles. Colors represent moisture probe readings (Volts). (C) Custom calibration to convert moisture tester and moisture probe readings to water content. Blue squares represent moisture tester readings. Red circles represent moisture probe readings. Blue and red solid lines represent calibration curves for the moisture tester and probe, respectively. Cyan and magenta dashed lines represent 68% confidence interval for future moisture tester and probe measurements, respectively. (D) Average moisture content as the number of misting cycles increase.

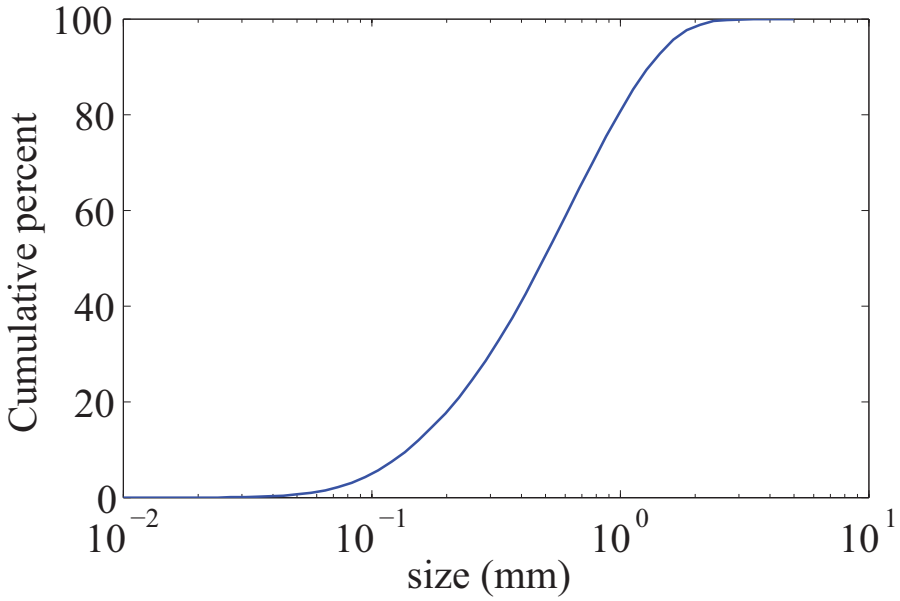

Figure 7. Cumulative grain size distribution of the sand used in the laboratory study (D_{50} = 0.56mm). Qualitatively, sand was fine to medium size with a small coarse size fraction overlying the main distribution.

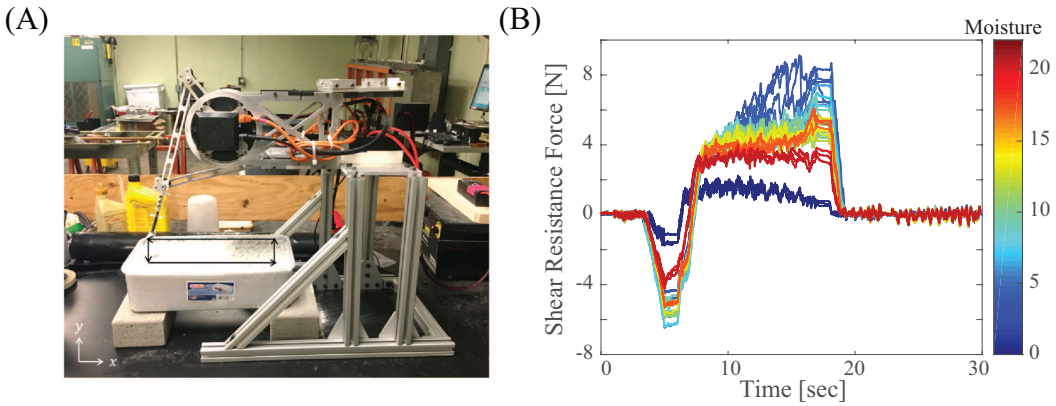

Figure 8. Experiment setup and measurements of the laboratory plowing tests. (A) Laboratory experiment setup. The direct-drive robotic leg was mounted on an aluminum frame, and performed continuous shear in a 30cm long, 11cm wide sandbox. Black arrows indicate the intruder trajectory during each trial. (B) Shear resistance force, F_x, recorded by the direct-drive leg for different moisture content. Color represents percentage of water content in the soil samples.

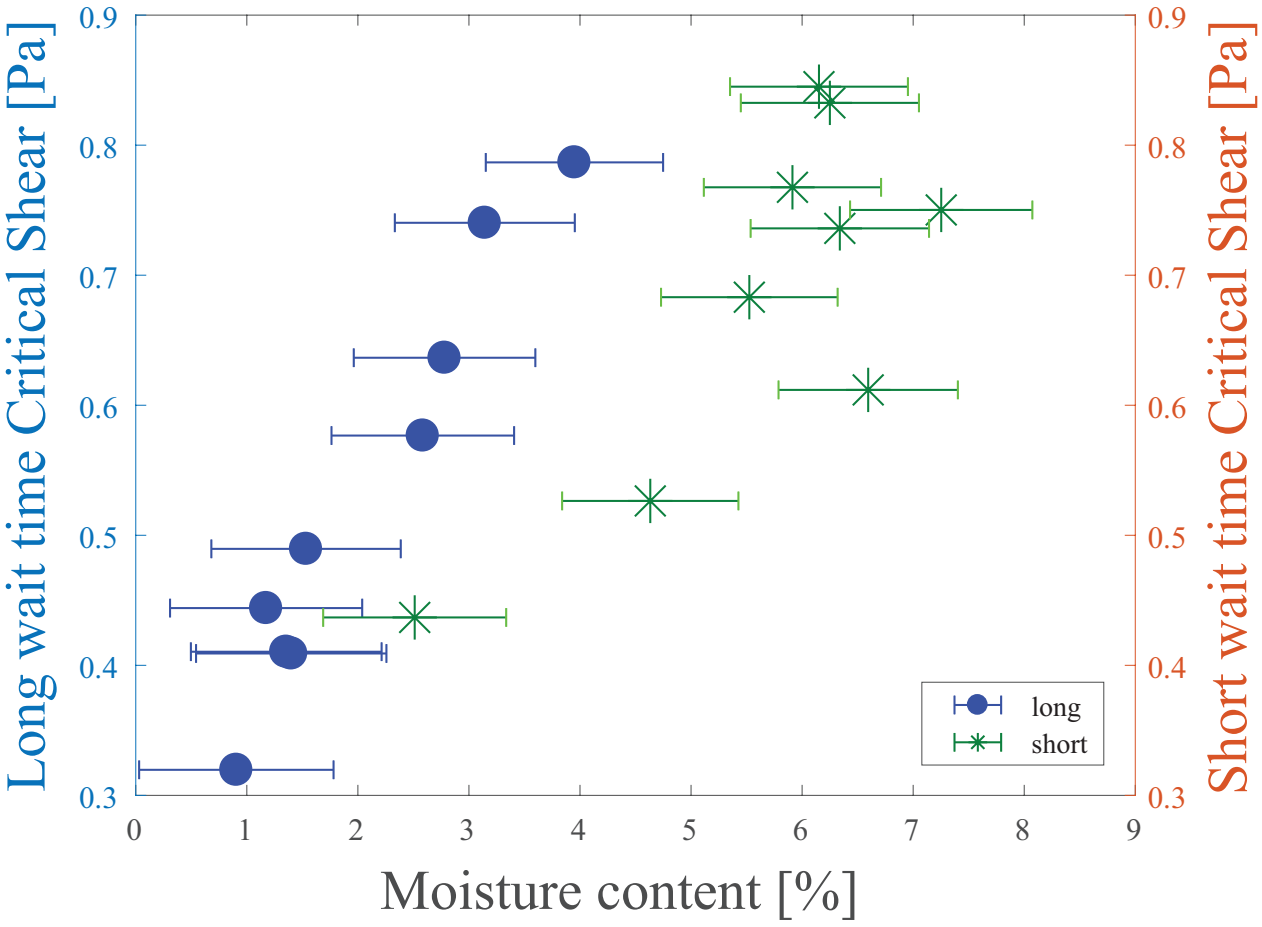

Figure 9. Infiltration time dependent differences in τ_c (estimated by the PI-SWERL) against surface moisture. Blue circles (long wait) depict τ_c for sand beds that have undergone infiltration times of 90 minutes or longer after wetting. Green stars (short wait) show τ_c for beds with infiltration times of 5 to 10 minutes. Error bars represent the 68% confidence interval of moisture measurements. Distinct groupings of the two measurements suggest that the τ_c of sand surface is controlled by subsurface saturation state as well as surface moisture.

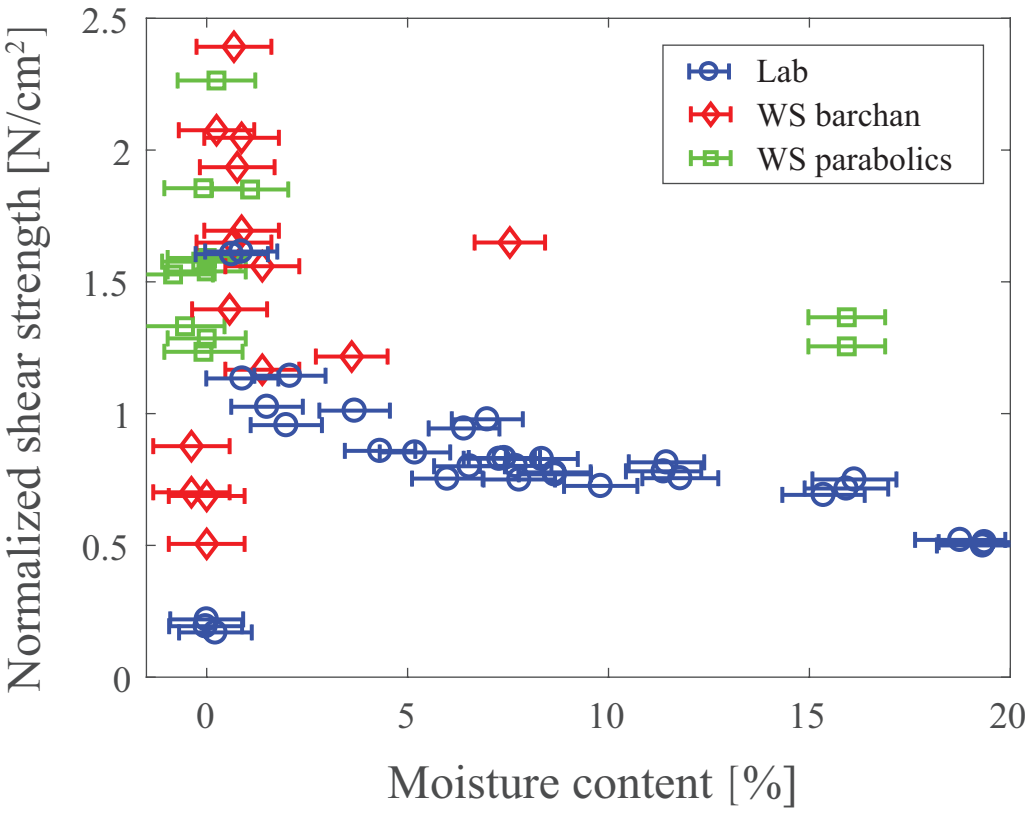

Figure 10. Normalized soil shear strength plotted as a function of moisture content. We define the normalized shear strength as the average shear resistance force normalized by the projected area of the plowing object perpendicular to the shear direction. Blue circles represent lab data where moisture content was systematically varied. Red diamonds and green squares represent field data in barchan and parabolic dunes at White Sands(WS), respectively. Moisture content for lab data was averaged from 3 different locations in the sandbox. Errorbar represent 68% confidence interval of moisture measurements.

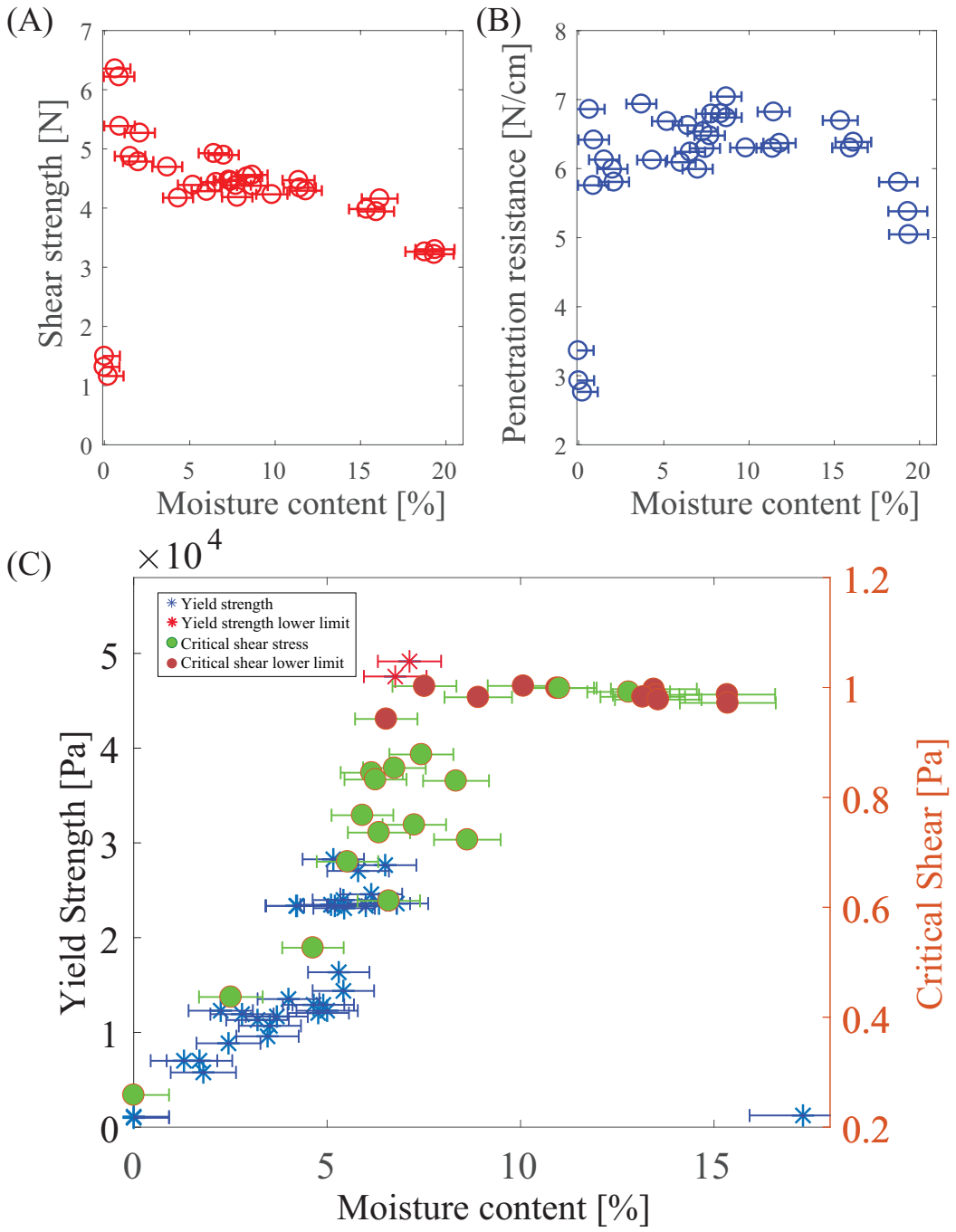

Figure 11. Erodibility characterized using different perturbation methods. (A) Average shear force measured in lab by the method described in Figure 3A. Error bars represent the 68% confidence interval of moisture measurements. (B) Penetration force per depth measured in lab by the method described in Figure 3C. Error bars represent the 68% confidence interval of moisture measurements. (C) A comparison of surface shear strength as measured by the test described in figure 3E and the estimate of τ_c provided by the PI-SWERL as described in Figure 3G. Stars represent yield strength, whereas circles represent critical shear stress τ_c. Error bars represent the 68% confidence interval of moisture measurements. From 0-6% the two appear to be roughly proportional. There is a jump in both τ_c and shear strength above 6 % moisture. This is evident by the lower limit points colored in red, which indicate that true measurements were unobtainable for the higher percent moisture values (with the exception of outliers in τ_c at 11 and 13 %). At the percent moisture corresponding to full saturation of the surface, the measured shear strength approaches its dry value.